A Thesis report on

Experimental Investigation on the Robustness Analysis of a Single-Link Flexible Manipulator towards Parametric Uncertainties and Input Disturbance

Submitted in partial fulfillment of the requirement for the award of degree of

MASTER OF ENGINEERING

IN

CAD/CAM

Submitted by

Amardeep Singh

(Roll no. 801584003)

Under the guidance of

Dr. Ashish Singla

Assistant Professor

Department of Mechanical Engineering

Thapar University, Patiala

DEPARTMENT OF MECHANICAL ENGINEERING

Thapar University

Patiala-147004, India

July, 2017

Declaration

I hereby declare that work done in this thesis entitled, **"Experimental Investigation on the Robustness Analysis of a Single-Link Flexible Manipulator towards Parametric Uncertainties and Input Disturbance"** submitted towards partial fulfilment of requirement for the award of degree of **Master of Engineering** in **CAD/CAM Engineering** at **Thapar University**, **Patiala**, is an authentic record of work carried out by me under the supervision of **Dr. Ashish Singla** (Assistant Professor, Mechanical Engineering Department, Thapar University, Patiala.)

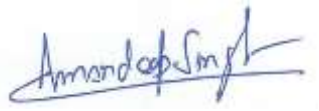

Date:17-07-2017

Amardeep Singh

Roll No. 801584013

This is to certify that above declaration made by the student is correct to the best of my knowledge and belief.

Dr. Ashish Singla

Assistant Professor

Mechanical Engineering Department

Thapar University, Patiala

Acknowledgements

Through this, I would like to thank the almighty God who blessed me with so many grateful moments and eminent personalities throughout my life. It's all started, when I first got familiar with one of the distinguished personality, **Dr. Ashish Singla**, during my Master's course in Thapar University, Patiala. Fortunately, after six months of my Master's course, I got the colossal opportunity to carry out my research work under his supervision.

I would like to acknowledge my guide **Dr. Ashish Singla,** (Assistant Professor, Thapar University, Patiala), for his benevolent propositions and positive guidance. His way of expressing the views on any topic inspires me a lot. They are all his amiable efforts who helped me in improving my soft skills along with research work. This work is a small tribute to show respect and admiration to him.

Further, I would like to show my deepest gratitude to **Mr. Jyotindra Narayan, Mr. Gaurav Garg and Mr. Ishan Chawla,** as my lab mates, for sharing quality ideas and having research oriented discussions. It was really blissful for being a part of such group having lot of diligence and smartness.

Moreover, I would like to acknowledge, **Mrs. Garima Sorahu**, **Mr. Kamaldeep Sharma, Mr. Gaganpreet Singh Hunjan** and **Mr. Jaspreet Singh,** as my colleagues, for their valuable advices at numerous choices making moments throughout my master's course. Also, I would like to them for balancing the humour in my tough times.

Further, I would like to acknowledge my parents, my beloved brothers, **Mr. Kuljinder Singh** and **Mr. Jaspreet Singh,** and my sister-in-law, **Mrs. Gurpreet Kaur** for their consistent support and motivations throughout my whole life. Finally, I would like to thank my friends, **Mr. Manu Dev Sharma, Mr. Liakatbir Singh** and **Ms. Harmandeep Kaur** for their noble suggestions and sparking stimulations in my life.

Amardeep Singh

Abstract

Over the last few decades, flexible manipulators are extensively used because of their light weight and low power consumption. However, reduction in weight of manipulator causes tip deflection. Many researchers used different controllers to eliminate tip deflection and implemented it on experimental model. Design of controller depends upon mathematical model of a system. The unmodeled dynamics of the system e.g. friction, backlash etc. leads to parametric uncertainties in the dynamic model, which are addressed in this thesis by designing robust controllers.

The first contribution of this thesis is to develop the accurate mathematical model, which is a prerequisite to design a suitable controller. Two approaches are used to develop the model of a single-link flexible manipulator: finite element method and lumped parameter method, by considering linear and angular tip deflection, respectively. Both the models are derived using Euler Lagrange approach. Mathematical models of the flexible manipulator are validated by comparing their step response with the step response obtained from Quanser experimental setup of single-link flexible manipulator. Linear Quadratic Regulator (LQR) and Integral Sliding Mode Controller (ISMC) are designed to control the tip deflection of the flexible manipulator. Gain of both the controllers are found by optimizing the weight matrices using Genetic Algorithms. Further, in this thesis, the performance of both the controllers are investigated on the basis of their robustness towards input disturbances. To investigate the effect of parametric uncertainties, different parameters associated with the manipulator such as mass, length, flexural rigidity and payload are varied and their effect on the manipulator frequency is reported. Moreover, the simulation results of both the controllers are compared with each other and are validated with the corresponding experimental results by applying input disturbances.

Table of Contents

List of Figures

List of Tables

List of Symbols

L	=	Length of the flexible link
m	=	Mass of the flexible link
I_l	=	Moment of inertia of the flexible link
D_b	=	Viscous friction coefficient of base
D_l	=	Viscous damping coefficient acting on the link
k_s	=	Stiffness of the link (rotational)
H	=	Damping energy
$\boldsymbol{x(t)}$	=	Generalized state vector
I_{hub}	=	Equivalent inertia at hub
$P.E.$	=	Potential energy
$K.E.$	=	Kinetic energy
$\boldsymbol{A_{lum}}$	=	State Matrix of FEM model
$\boldsymbol{B_{lum}}$	=	Input Matrix of FEM model
$\boldsymbol{u(t)}$	=	Input vector of state space
i	=	Node of the beam
n	=	Number of elements of the flexible link
(u_{2i-1})	=	Displacement of i^{th} element
(u_{2i})	=	Slope of i^{th} element
$\boldsymbol{u^p}$	=	Local displacement vector of element

$y(x,t)$	=	Displacement within element of beam
l	=	Length of the element
$\boldsymbol{M^e}$	=	Mass element of matrix
K	=	Potential energy of element
$\boldsymbol{K^e}$	=	Stiffness matrix of element
E	=	Young's Modulus
$\boldsymbol{u^g}$	=	Global displacement vector of cantilever beam
$\boldsymbol{K^g}$	=	Global stiffness matrix of cantilever beam
$\boldsymbol{M^g}$	=	Global mass matrix of cantilever beam
T_j	=	Kinetic energy of element
$\boldsymbol{M}$	=	Mass matrix of the flexible link
$\boldsymbol{M(q)}$	=	Symmetric positive-definite inertia matrix
$\mathbf{n}(\mathbf{q},\dot{\mathbf{q}})$	=	Vector of Coriolis, centripetal, gravitational and elastic forces
$\boldsymbol{M_l}$	=	Mass matrix of the flexible link in equation of motion
$\boldsymbol{N_l}$	=	Damping matrix of the flexible link in equation of motion
$\boldsymbol{G_l}$	=	Stiffness matrix of the flexible link in equation of motion
K_g	=	Reduction ratio of motor shaft to load shaft
R_m	=	Armature resistance of motor
K_m	=	Torque constant of motor
V_m	=	Voltage of motor

$\boldsymbol{C_f}$	=	Controllability matrix
$\boldsymbol{Q}$	=	State weighting matrix
$\boldsymbol{R}$	=	Control cost matrix
$\boldsymbol{u}$	=	Input of the flexible manipulator
$\boldsymbol{x}$	=	Variable vector of the flexible manipulator
$\boldsymbol{x_d}$	=	Desired vector of the flexible manipulator
J_o	=	Cost function of the controller
$\boldsymbol{K}$	=	Gain of the controller
e_θ	=	Error in of shaft angle
e_α	=	Error in tip deflection
$\boldsymbol{g(x,t)}$	=	Input disturbance vector
$\boldsymbol{u_d}$	=	Input disturbance
u_0	=	Input from the controller without disturbance
$\boldsymbol{G}$	=	Projection matrix
$\boldsymbol{u_0}$	=	Discontinuous control input
$s(x,t)$	=	Sliding surface of the dynamic system
M_0	=	Sliding Mode Constant
$\boldsymbol{A_{fem}}$	=	State Matrix of FEM model
$\boldsymbol{B_{fem}}$	=	Input Matrix of FEM model
θ	=	Shaft angle

τ	=	Torque applied at shaft
α	=	Angular tip deflection
$\mathcal{L}$	=	Lagrange polynomial of the system
$\dot{\theta}$	=	Angular velocity
$\ddot{\theta}$	=	Angular acceleration
$\dot{\alpha}$	=	Tip deflection velocity
$\ddot{\alpha}$	=	Tip deflection acceleration
τ	=	Torque at shaft
ϕ_i	=	Shape function
ρ	=	Mass per unit length
η_g	=	Gear box efficiency of motor

Chapter 1

Introduction

1.1. Manipulator

A manipulator is used to manipulate materials without having direct contact. Primarily, the applications made use of robotic arms to deal with radioactive material. Nowadays, they are used in variety of applications such as surgery assisted by robots, welding automation and in space. It has an arm-like mechanism with segments' series, usually jointed and sliding (called cross slides), that holds and shift the objects through a number of degrees of freedom. In industries, a manipulator is used as an assisting device to lift and place the articles that are large, heavy or hot. Manipulator tooling helps the lift to roll or spin the parts and appropriately place them as well as it has the ability to reach into tight places, for lifting purpose. Manipulator can be used for various applications in industries like pick and place, assembly, welding, paint etc. A rigid manipulator installed at GNA Axles is shown in Figure 1.1. It is observed that these manipulators are very bulky in nature, leads power consumption in moving the object from one location to other. Moreover, their speed of operation speed is reasonably low. To address these two issues, the trend is towards making light-weight manipulators. With reduction in mass, tip position instability occurs and this problem is solved developing suitable controllers.

Figure 1.1: Rigid manipulator

1.2. Flexible Manipulator

The reduction in the weight of the manipulator decreases its stiffness, which causes tip deflection and makes it flexible in nature. Flexible manipulator stores two types of potential energies, due to position of the link and due to stiffness of the link. The potential energy due to stiffness causes tip deflection. On other hand, the rigid manipulator has very high stiffness and thus it stores the potential energy, mainly due to the position of the link in the gravitational field. A single-link flexible manipulator, developed by Quanser (Canada) is shown in Figure 1.2.

Figure 1.2: Quanser flexible manipulator

Flexible manipulator has a number of advantages over its rigid counterpart, which are as given below:

- Large work volume
- Low cost price
- Large amount of payload to manipulator weight ratio
- Higher operational speed
- Low power actuators
- Easily transportable
- Lesser energy consumption
- Reduced inertia leads to safe operations

However, flexible manipulator has a big disadvantage that the vibrations are more due to low stiffness.

However, the trajectory and the position control of the flexible manipulator is a very challenging task.

1.3. Applications of Flexible Manipulators

The flexible manipulators have a variety of applications. Some of the applications are listed below:

- Aerospace Industries: To reduce the launching cost of space missions by minimizing the weight of robots as well as by minimizing energy using lower weight manipulators[1]–[3]. Space manipulator is shown in Figure 1.3.

Figure 1.3: Flexible manipulator in space [W1]

- Nuclear Power Plants: Manipulators can be used in higher radiation areas and nuclear waste disposal to protect and help the nuclear workers[4].
- Medical Surgeries: Flexible manipulators can be used in hospitals to perform operation to overcome the present robotic systems that are expensive and bulky. The flexible manipulator can be easily used for internal inspection of the body[5].
- Military: Flexible manipulators can be used for inspection, diffusion of bombs as they can easily reach through the gaps due to their flexibility. Figure 1.4 represent man carrying light weight flexible manipulator (Bulle) to inspect military aircrafts.

Figure 1.4: Man carrying flexible manipulator in backpack to inspect military aircraft. [W2]

- Commercial Industries: Flexible manipulators can be used in commercial industries to reduce the production cost[6].

1.4. Objective of Thesis

The objectives of the proposed work are listed below:

- Modeling of the flexible manipulator is done by using finite element method and lumped parameter method.
- Actuator dynamics are augmented with both the models.
- Genetic Algorithm based linear quadratic regulator is designed to minimize the tip deflection.
- Integral sliding mode controller is also design to compensate input disturbance.

1.5. Organization of Thesis

The Present dissertation is organized as follows-Chapter 2 represents the detailed literature survey of the flexible manipulator system. The survey starts, with the modeling of the flexible manipulator, where different modeling techniques used by researches are discussed. Further, the controllers used by researches to address the tip deflection problem of flexible manipulator are discussed.

Chapter 3 deals with mathematical modeling of flexible manipulator. Two methods are used to develop dynamic model of flexible manipulator; finite element method by considering linear tip deflection and lumped parameter model by considering angular tip deflection. The

actuator dynamics is augmented with flexible link manipulator for better accuracy. Furthermore, the real time apparatus, Quanser flexible manipulator

Chapter 4 presents two controller techniques i.e. linear quadratic control and integral sliding mode control, to minimize the tip deflection while tracking shaft angle. Further, study of these controllers for input disturbance is presented.

Chapter 5 explains the experimental setup of the flexible manipulator and its components. The parameters considered for the experimental setup is presented in this chapter. The validation of the mathematical model and controlling technique is performed using this apparatus.

Chapter 6 presents comparative analysis of two mathematical models i.e. finite element method and lumped parameter method with real time apparatus. The frequency analysis of dynamic system is done on finite element model for length of the link, mass of the link, flexural rigidity and payload. Furthermore, weight matrices are optimized by genetic algorithm and compared with hit and trial method.

Chapter 7 presents the major report of the thesis work. Furthermore, future work is also suggested in this chapter.

Chapter 2

Literature Review

2.1. Introduction

In this Chapter, a literature survey of the modeling and control of flexible robotic manipulators is presented. The study on the control of a flexible arm manipulator started as a part of the space robotics research. The space manipulator should be as light as possible in order to reduce its launching cost. *Book* [7] had illustrated about the manipulator for space application. It is important to consider the link flexibility in the modeling of a manipulator. The advantages and shortcomings of different methods applied by the researchers for analyzing the flexibility of a link are discussed in this section. Further, modeling and control section are classified according to the techniques utilized. An effort has been made to survey the works of different researchers in this field. Extensive literature reviews, in the same field, are presented by *Dwivedy and Eberhard* [8] in 2006, by considering different methods of modeling and control. In 2013, *Kaing et al.* [9] had discussed various techniques to control the vibrations of a flexible manipulator. The detailed literature survey is categorized as given in Figure 2.1.

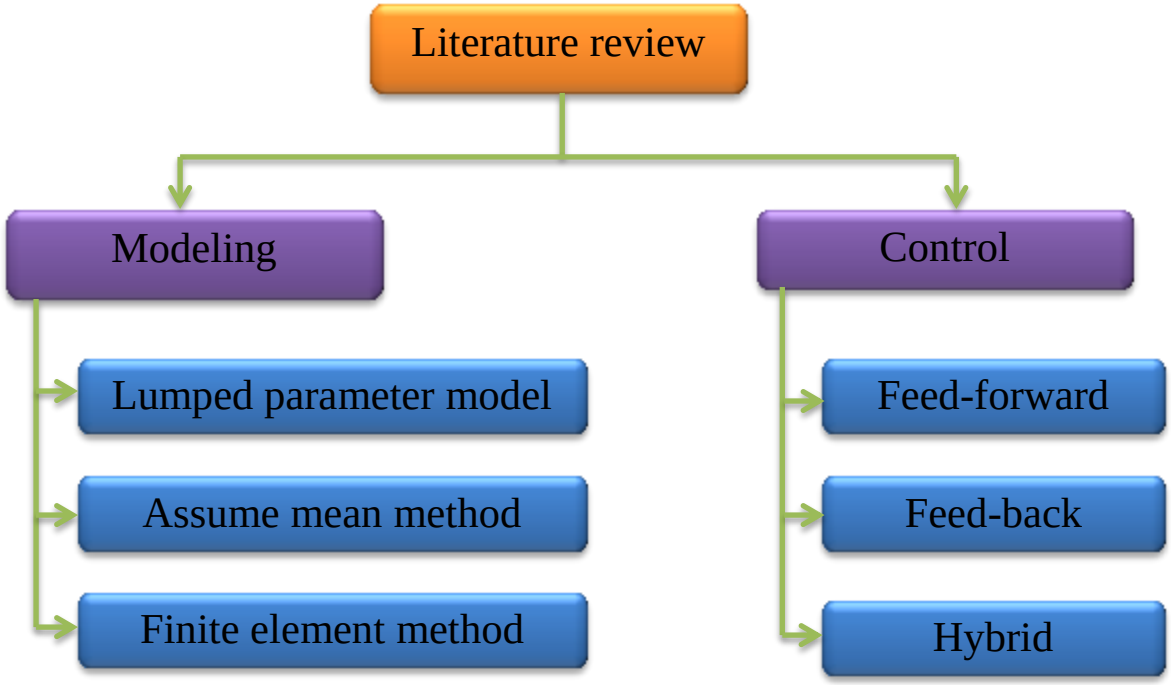

Figure 2.1: Layout of Literature review

2.2. Modeling of Flexible Manipulators

A literature review of the modeling of the flexible manipulator is carried out in this section. Contribution of the different researchers in the modeling category are grouped together as assumed mean mode, lumped parameter model, finite element model.

2.2.1. Assumed Mode Method (AMM)

In this method, spatial mode eigenfunctions and time-varying mode amplitudes are used to represent the flexibility of the link which is truncated into finite model series. Truncation of cantilever beam by assumed mode method is shown in Figure 2.2.

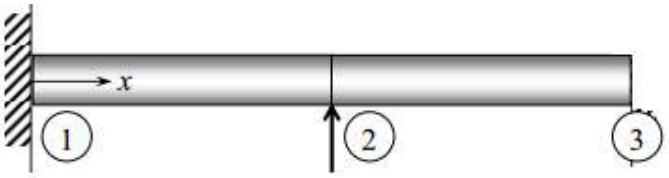

Figure 2.2: Series discretization of beam [W3]

In 1981, *Book and Hastings* [7] demonstrated assumed mean method to formulate the linear dynamic equations of the flexible link and the comparative analysis of model simulation measurement was performed with 4 feet long drive arm real model. In 1989 *Book et al.* [10] presented the verification of system model by using assumed mode method. Moreover, authors also compared the calculated eigenvalues and eigenvectors by real-time frequency and their respective mode shapes. In 1990, *Belleza et al.* [11] utilized exact eigenfunction, by using pseudo-clamped and pseudo-pined boundary conditions, for the flexible manipulator. Thereafter, the author also considered the payload and hub inertia in the modeling of the system. *Theodore and Ghosal* [12] compared the assumed mean mode and the finite element method, for modeling the system. Meanwhile, authors concluded few calculations that are required to obtain mass and stiffness matrix in finite element method as compared to the assumed mean mode method. However, the number of equations of motion that is derived in the finite element method is more. It is concluded from literature survey that assumed mean method for the uniform cross-section of the flexible link and for the non-uniform cross-sectional area, finite element method must be used. However, in modeling of more than one link manipulator, finite element method is preferred over the assumed mean mode method for any cross-section. In 1993, *Matsuno et al.* [13] discussed the optimal input torque and trajectory of the robot with three degrees of freedom, whose last link is flexible in nature to

maintain the minimal torque so that vibration of the system is minimum. *Karray et al.* [14], *Rakhsha and Goldenberg* [15], *Barbieri and Ozguner* [16] also used assumed mean mode method to model the dynamics of the system and implemented a hybrid controller to control the vibration of the system.

2.2.2. Lumped Parameter Method (LPM)

In the lumped parameter model, which is the simplest one for analysis purpose, the manipulator is taken into consideration for modeling as spring and mass system. The lumped parameter model does not often yield accurate results, sufficiently. Figure 2.3 shown a lumped parameter model.

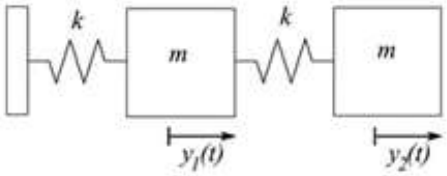

Figure 2.3: Beam discretization using lumped model [W4]

Zhu et al.[17] had modeled a system in a very easy manner by considering a massless spring of length same as link length and summed up the payload mass and spring equivalent mass at the tip of the model. *Raboud et al.*[18]used the lumped parameter approach to model a cantilever beam by varying the payload and different aspect ratio of a cross-section which concluded that more than one equilibrium point exists in case of the flexible link. *Megahed and Hamza* [19] considered a lumped parameter model and element near the revolute joint that are taken as a rigid body to formulate the problem. By using the numerical simulation, they showed that the ignorance of the link rigidity at connection may introduce large error and also proposed the consistent mass matrix in order to better approximate the model. *Popescu et al.* [20] in 2008, introduced the lumped parameter model for implementation of the hybrid controller to control the vibration quanser flexible beam. *Khalil and Gautier*[21] model mechanical system with lumped elasticity. *Nissing* [22]optimize value of spring constant and damping to obtain fast response of robot.

2.2.3. Finite Element Method (FEM)

FEM splits a large problem into smaller and simpler parts called finite elements, as shown in Figure 2.4. The simple equations that model these finite elements are then assembled into a larger system of equations that models the entire problem. Each element in the system has its

own potential and kinetic energy. Then, these elements are combined together to formulate the expression for kinetic and potential energy for the whole system.

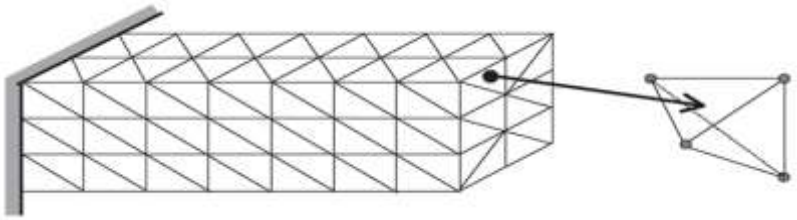

Figure 2.4: Discretised beam using finite element method [W5]

In 1986, *Usoro et al.* [23] utilized the kinetic energy and potential energy of the system to calculate the lagrange polynomial and formulated dynamic equation of the system using lagrange approach. *Theodore and Ghosal* [12] had done comparative analysis with the assumed mean method and finite element method for modeling the system. In 1997 *Tokhi et al.* [24] made a comparison between the finite difference and finite element approach on the basis of accuracy and computational speed. However, it is concluded that the finite element model is more complex than finite difference method while better accuracy and performance is achieved using the finite element approach. In 1999 *Tokhi and Mohamed* [25] presented the evolution of performance by varying the number of nodes in the dynamic finite element modeling of the flexible link. The computational time for the problem increases by increasing the number of nodes while the model of accuracy increases. In 2005 *Martins et al* [26] , three different approaches had been presented for modeling by using assumed mean mode with linear displacement and quadratic displacement and the third one by using finite element method. Complete validations regarding these three models had been done by using time-domain and frequency-domain. In 2004 *Mohamed and Tokhi* [27], used finite element model of the flexible manipulator for comparison of the input shaping and input filtering technique to control the vibrations in the flexible manipulator. *Singla et al.* [28], [29] had illustrated finite element model to control the vibration of the system using a hybrid controller which is a combination of feed-forward and feedback techniques. *Nagarajan and Turcic* [30], *Alberts et al* [31] also works on finite element model to conduct their experiment on flexible link.

2.3. Control of Flexible Manipulators

After obtaining the accurate and precise model of the flexible system, furthermore the construction of a controller is another challenge. There are several schemes such as feed-forward, linear quadratic regulator, self-tuning control, adaptive control, PID regulator, to

control the vibration of the flexible manipulator. Earlier in late 19th-century researchers, the main focus was to develop an accurate dynamic model of the flexible manipulator but nowadays they prefer more on control strategies rather than modeling. An effort is made to group the different control strategies. The advantages and disadvantages of the controller are discussed in Table 1.1.

2.3.1. Feedforward Control

In feedforward control, the angular position, angular velocity, and angular acceleration are given and calculation of required torque is done to obtain the desire motion of an arm. Feed-forward control is very helpful where the repetitive operation is required. Response to the feed-forward control is very fast. In 1993 *Mutsuno et al.* [13] discussed the optimal torque requirement and optimal trajectory following in handling of the flexible beam by two-link manipulator. *Park* [32] optimized the path of two-link flexible manipulator so the residual vibration of the link is minimal. Fourier series and polynomial were combined together, with a harmonic coefficient of each so that vibrations are minimized. In 2009, *Abe* [33] expressed the joint angle as a cubic spline function and particle swarm technique is used to optimize the path trajectory for minimum vibrations. *Choi et al.* [34] offered a smooth state trajectories irrespective of poles and dynamics of the system achieved by equilibrium manifold express as an exponential function. Some researchers also attained feed-forward control of a plant with command Shaping. Command Shaping is a control method for decreasing vibrations in the system. The method works by producing a command signal that scratches its own vibration. That is, vibration produced by the first command signal is annulled by vibration caused by the second command. The method involves the convolution of the reference input. The shaped command that derived from the convolution is then used as the input of the system. If the impulses in the shaper are selected properly, then the systems will not vibrate to any unshaped command. The amplitudes and time locations of the impulses are obtained from the system's natural frequencies and damping ratios. *Rhim and Book* [35] presented a command shaping method using commuted shaping order technique for both single mode and multi-mode system. *Mohamed et al.* [27] utilized input shaping, low-pass and band-stop filtered input techniques to diminish the vibration of flexible manipulator. Figure 2.5 represents both feedforward and feedback controller.

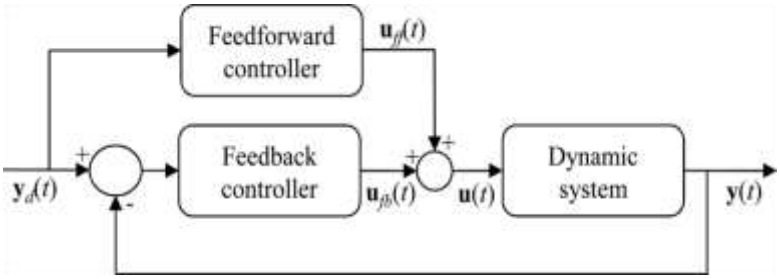

Figure 2.5: Block diagram of feedforward controller and feedback controller [W6]

2.3.2. Feedback Control

In feedback control, the signal to be controlled is compared to the desired reference signal through the comparator. Thus, the comparator generates the error signal. The error is used to compute corrective control action, by the controller on the plant. In 1986, *cannon and Schmitz* [2] made an initial attempt to control the vibrations of system by applying feed-back control on the tip position of the flexible manipulator. *Shuzhi et al.* [17] used the non-linear strain based feed-back signal to control the tip position of the flexible link. *Karray et al.* [14] proposed the robust controller technique by using the sliding mode control combined with another controller to improve tip tracking of the flexible manipulator. *Song et al.* [36] had worked on the robustness of position based vibration control for single mode as well as multimode Vibration suppression. *Orszulik and Shan* [37] used the recursive least square method to drive the adaptive parameter estimator and with help of these parameters, position feedback controller is designed. *Gurses et al.* [38] used PD controller to control the hub angle and PZT actuator attached on the surface of flexible link. PZT actuator is used for vibration suspension by compensating linear and angular velocity. PD controller is exploited by *Zhu et al.* [39] on a dynamic system modeled by lumped parameter model. *Kotnik et al.* [40] use acceleration feedback to control manipulator. *Wang and Li* [41] design an integrated of sensing and filtering for a single link flexible manipulator.

2.3.3. Hybrid Control

Hybrid controller is the amalgamation of both feed-forward and feed-back controller. In Hybrid Control, the shortcomings of an existing controller are compensated by using another controller in addition to it. *Lew and Book* [42] build hybrid controller for flexible manipulator. *Mohamed et al.* [43] build a hybrid controller using command shape and PD to control the vibrations. In this paper, the gain of the PD controller was optimized using the Genetic algorithm. *Singla et al* [28] modeled a hybrid controller by combining the PD controller, reduce order observer and command shaping. Linear Quadratic Regulator is the

optimal control that is used to minimize the cost associated with generating control inputs. The cost function consists of two matrices, Q and R, that are state weighting matrix and control cost matrix. For a linearized plant, the objective of LQR controller is to minimize the integration of sum of these two matrices from initial to final time by using a feedback regulator. *Lee and Lee* [44] design a hybrid controller for tracking problem oh two link manipulator. *Etxebania et al.* [45] made a comparison between linear quadratic regulator and adaptive sliding mode controller. *Mohamed et al.*[46] used hybrid controller that is the combination of the linear quadratic regulator and another controller. *Singla et al* [29] modeled a hybrid controller by combining the linear quadratic regulator to achieve zero stability error, reduce order observer to estimate non-measurable quantities, command shaping for lessening the vibration level.

Table 1.1: Comparison between Different Controllers

Controller	Advantages and Disadvantages
Feed-forward	Advantages • Because of no need of sensor, it is economical Disadvantages • It is impossible to neglect Non-linearity. • Small disturbance and change in parameter is difficult to handle by the controller
Feed-back	Advantages • Adaptable to the system changes • In the case of endpoint acceleration as a feed-back, high-frequency feed-back results in good vibration suspension. • Grantee stability. Disadvantages • Difficult to tune for more than one mode of vibration. • In some cases, high control effort may require.
Linear quadratic control	Advantages • Easy to tune • Effort requires to control is minimal. • Provide zero stability error. • It can solve non-linear system. Disadvantages

	• It can applied be only to system using full state feed-back
Command Shaping	Advantages • It does not use any sensor therefore economical. • It cancels the vibration instance immediately when it is produced, therefore no vibration can be possible. • It converges more rapidly. Disadvantages • A dynamic model of the system should be accurate.

2.4. Conclusions from Literature Review

Through the literature review in which the works reported by many authors on dynamics modeling and control strategies for flexible manipulator, following observations are drawn.

- The precision of dynamic modeling of the system plays an important role in tackling the problem. Most of the authors reported various mathematical model techniques to find out the system dynamics formulations of the flexible manipulator. Many authors had not considered the actuator dynamics, which can play a vital role in the modeling of the flexible manipulator system.
- Dynamic modeling using assumed mode method requires more computation than finite element method. However, assumed mean mode is more precise than finite element method for single link manipulator whereas, for the multilink flexible system, finite element method provides a more efficient dynamic model.
- Most of the researchers consider the angular motion of the shaft and linear tip deflection while modeling the flexible manipulator.
- By increasing the number of node in truncation of the system, accuracy of dynamic model increases. Moreover, it induces the higher frequency modes and more computational time of the system.
- Validation of the model can be done in two ways. First is frequency-domain validation where the comparison of natural frequency for the two different models is performed and the second is time-domain validation which is performed by comparing the response of the model to singularity functions. Most of the mathematical model validations are done by comparing the natural frequency of the model with the natural

frequency of the real-time model or natural frequency of model available in the literature.

- In late 19^{th} century and earlier period of the research, researchers focused on the dynamic modeling of system and used the simple technique to control the vibrations of manipulator. Nowadays many researchers are using the hybrid controller technique because basic dynamic model is not so precise. Very few hybrid controllers are implemented on the real-time system of a flexible manipulator.
- In deriving the mathematical model, there are always some factors which are assumed, thus there is need of controllers which are not sensitive to the inaccurate mathematical model and parameter uncertainties.
- Few work is also done in the field of intelligent control of flexible manipulator. Many researchers optimize the feed-forward control input by using various optimization techniques. Moreover, optimization of the feed-back gain of PD controller is also shown in few research papers. Although, LQR is an optimization and robust technique further there is a room for optimization in the selection of weight matrices.
- Command shaping is cheaper controlling method than the feed-back controls because it does not require a sensor. Controller used in combinations with other controller performs better than working on its own. Although, this may lead to increase in the cost of control of the system.

In this thesis, mathematical modeling of the flexible manipulator is performed in two different ways. The first one is finite element method by considering the angular motion of the shaft and linear tip deflection, whereas the second one is lumped element method by taking the angular motion of the shaft and angular tip deflection in consideration. Euler-Lagrange method is used to compute both the models. Further, actuator dynamics are augmented with both the models. To validate these models time-domain analysis of models is performed with the real-time model. LQR and ISMC controller are used to minimize the tip deflection. Moreover, Genetic algorithm (GA) as an optimization and search tool is used to determine the optimum value of weight matrices in LQR controller. Thereafter, both the controllers are compared for input uncertainty which is the key consequence of input noises.

Chapter 3

Modeling of Flexible Manipulators

3.1. Introduction

Before implementation of control, it is important to derive an accurate mathematical model. Many computational software such as SolidWorks, SimMechanics, Simwise 4D, Bond graph etc. are available to compute the dynamics of any system. Three different mathematical methods to model the flexible link were discussed in Chapter 2. In this section, two approaches are used to model the system dynamics i.e. lumped parameter and finite element method. Moreover, after discretization using above mention techniques, two approaches are typically used to solve the dynamics of the system i.e. Newton-Euler approach based on force/moment balance and Euler-Lagrange approach based on the energy balance, for calculating the equations of motion. Euler-Lagrange method is comparatively easy to compute for complex system and system having a high degree of freedom. Therefore both the models are computed using Euler-Lagrange approach.

3.2. Lumped Parameter Method

In this method, the flexible link is being considered as a Euler-Bernaulli beam, which is modeled as a simple spring-mass system. The flexible link model is shown in Figure 3.1. The base of the flexible link is mounted on the actuator system. Whenever the rotation of actuator is in the counter-clockwise (CCW) direction, the servo angle, θ, positively rises.

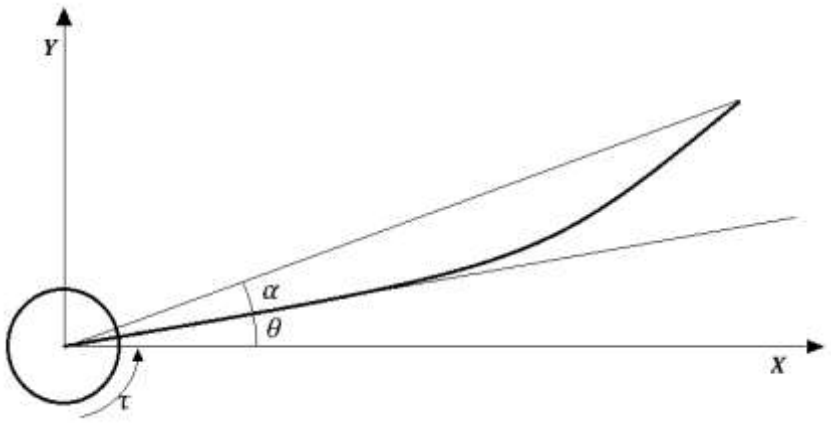

Figure 3.1: Schematic diagram of flexible link for Lumped Parameter Modeling

The flexible link has a total length of l, a mass of m, and its moment of inertia about the axis of rotation is I_l. The link deflection angle is designated as α and rises positively, if CCW rotation is considered. The input, torque τ, rotates the base of the link. The viscous friction coefficient of base is D_b. This is the friction that works against the torque being smeared upon the hub or base of link. The friction acting upon the link is represented by the viscous damping coefficient D_l. Finally, the flexible link is considered for modeling as a linear spring having stiffness k_s.

Total potential stored in the system is given by Equation (3.1),

$$P.E. = \frac{1}{2} k_s \alpha^2 \tag{3.1}$$

Total kinetic energy regarding the system is sum of kinetic energy of the hub and the link which is given by Equation (3.2),

$$K.E. = \frac{1}{2} I_{hub} \theta^{\cdot 2} + \frac{1}{2} I_l (\theta^{\cdot 2} + \alpha^{\cdot 2}) \tag{3.2}$$

Lagrange polynomial of the system is given by the subtraction of kinetic energy and potential energy that can be represented as given in Equation (3.3):

$$\mathcal{L} = K.E. - P.E. \tag{3.3}$$

From Equation (3.1) and (3.2), Lagrange polynomial can be derived as given in Equation (3.4),

$$\mathcal{L} = \frac{1}{2} I_{hub} \theta^{\cdot 2} + \frac{1}{2} I_l \left(\dot{\theta}^2 + \dot{\alpha}^2\right) - \frac{1}{2} k_s \alpha^2 \tag{3.4}$$

Heat or damping polynomial H is given by Equation (3.5),

$$H = \frac{1}{2} D_b \theta^{\cdot 2} + \frac{1}{2} D_l \alpha^{\cdot 2} \tag{3.5}$$

Due to two generalized coordinates, there are two equations of motion of the system. Therefore, Lagrange's equations of the system can be written as Equation (3.6) and (3.7),

$$\frac{d}{dt}\left(\frac{\partial \mathcal{L}}{\partial \dot{\theta}}\right) - \frac{\partial \mathcal{L}}{\partial \theta} + \frac{\partial H}{\partial \dot{\theta}} = \tau \tag{3.6}$$

$$\frac{d}{dt}\left(\frac{\partial \mathcal{L}}{\partial \dot{\alpha}}\right) - \frac{\partial \mathcal{L}}{\partial \alpha} + \frac{\partial H}{\partial \dot{\alpha}} = 0 \tag{3.7}$$

After solving the Equations (3.6) and (3.7), the Equation (3.8) and (3.9) of motion are obtained.

$$(I_{hub} + I_l)\ddot{\theta} + I_l\ddot{\alpha} + D_b\dot{\theta} = \tau \tag{3.8}$$

$$I_l\ddot{\theta} + I_l\ddot{\alpha} + B_l\dot{\theta} + K_s\alpha = 0 \tag{3.9}$$

By writing the Equations (3.8 and 3.9) of motions in matrix form given by Equation (3.10),

$$\begin{bmatrix} I_{hub} + I_l & I_l \\ I_l & I_l \end{bmatrix}\begin{bmatrix} \ddot{\theta} \\ \ddot{\alpha} \end{bmatrix} + \begin{bmatrix} D_b & 0 \\ 0 & D_l \end{bmatrix}\begin{bmatrix} \dot{\theta} \\ \dot{\alpha} \end{bmatrix} + \begin{bmatrix} 0 & 0 \\ 0 & k_s \end{bmatrix}\begin{bmatrix} \theta \\ \alpha \end{bmatrix} = \begin{bmatrix} \tau \\ 0 \end{bmatrix} \tag{3.10}$$

Therefore,

Matrix of inertia forces, $$\boldsymbol{M_l} = \begin{bmatrix} I_{hub} + I_l & I_l \\ I_l & I_l \end{bmatrix} \tag{3.11}$$

Matrix of damping forces, $$\boldsymbol{N_l} = \begin{bmatrix} D_b & 0 \\ 0 & D_l \end{bmatrix} \tag{3.12}$$

Matrix of gravitational forces, $$\boldsymbol{G_l} = \begin{bmatrix} 0 & 0 \\ 0 & k_s \end{bmatrix} \tag{3.13}$$

The dynamic model, given in Equation (3.10) can be represented in the standard state space by taking generalized state vector $\boldsymbol{x(t)} = [\theta\ \alpha\ \dot{\theta}\ \dot{\alpha}]$ as in Equation (3.14),

$$\dot{\boldsymbol{x}}(\boldsymbol{t}) = \boldsymbol{A_{lum}x(t)} + \boldsymbol{B_{lum}u(t)} \tag{3.14}$$

where, $$\boldsymbol{A_{lum}} = \begin{bmatrix} \boldsymbol{0_n} & \boldsymbol{I_n} \\ -\boldsymbol{M_L^{-1}G_L} & -\boldsymbol{M_L^{-1}N_L} \end{bmatrix} \quad \text{and} \quad \boldsymbol{B_{lum}} = \begin{bmatrix} \boldsymbol{0_n} \\ \boldsymbol{M_L^{-1}} \end{bmatrix} \tag{3.15}$$

3.3. Finite Element Method (FEM)

To find the dynamic equation of flexible beam first step is solve the dynamics of a cantilever beam by using Euler-Bernoulli theory [47]. After, formulating the equation of motion in case of the cantilever beam, in next section, the equation of motion concerning the Flexible Link is to be find out.

3.3.1. Mass and Stiffness Matrix of Cantilever Beam

The cantilever beam is truncated into, n linear elements having two nodes. i^{th} node of the beam has two degree of freedom that is transverse displacement (u_{2i-1}) and slope (u_{2i}). u^p is the local displacement vector for the element of beam.

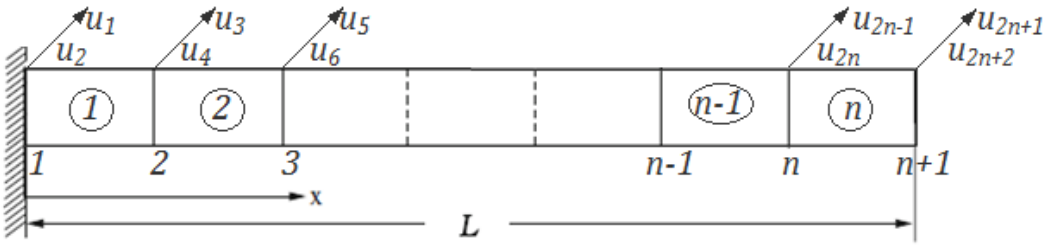

Figure 3.2: Discretization beam using finite element

$$\boldsymbol{u^p} = [\, u_1\, u_2 u_3\, u_4\,]^T \tag{3.16}$$

The displacement within element $y(x,t)$is represented by Equation (3.17),

$$y(x,t) = \sum_{i=0}^{4} \phi_i(x) u_i(t) \tag{3.17}$$

where, ϕ_i is the shape function. The prescribe boundary conditions of element are given in Equation (3.18),

$$\begin{aligned} &\text{At } x = 0, && y(0,t) = u_1, && \frac{\partial y(0,t)}{\partial t} = u_2 \\ &\text{At } x = l, && y(0,t) = u_3, && \frac{\partial y(0,t)}{\partial t} = u_4 \end{aligned} \tag{3.18}$$

There are four constraints on each element, therefore cubic polynomial with four constant can be used as a shape function ϕ_i, given by Equation (3.19),

$$\phi_i = a_i + b_i x + c_i x^2 + d_i x^3 \;\; \forall \;\; i = 1,2,3,4 \tag{3.19}$$

Constant can find out by solving the Equation (3.17) against the boundary condition of shape function which can be derived from boundary condition of elements which is also known as Hermite-polynomials [47].

$$\phi_1 = 1 - 3\frac{x^2}{l^2} + 2\frac{x^3}{l^2}$$

$$\phi_2 = x - 2\frac{x^2}{l} + \frac{x^3}{l^2}$$

$$\phi_3 = 3\frac{x^2}{l^2} - 2\frac{x^3}{l^2}$$

$$\phi_4 = -\frac{x^2}{l} + \frac{x^3}{l^2} \tag{3.20}$$

Substituting Equation (3.20) into Equation (3.17), the Equation (3.21) is formulated which gives us the transverse deflection of the beam element.

$$y(x,t) = \left(1 - 3\frac{x^2}{l^2} + 2\frac{x^3}{l^2}\right)u_1 + \left(x - 2\frac{x^2}{l} + \frac{x^3}{l^2}\right)u_2 + \left(3\frac{x^2}{l^2} - 2\frac{x^3}{l^2}\right)u_3 + \left(-\frac{x^2}{l} + \frac{x^3}{l^2}\right)u_4 \tag{3.21}$$

Equation (3.22) evaluates the kinetic energy of a single element.

$$K.E. = \frac{1}{2}\int_0^l \rho(x)[\dot{y}(x,t)]^2 dx \tag{3.22}$$

Using Equation (3.17) kinetic energy can be derived as given in Equation (3.23),

$$K.E. = \frac{1}{2}\int_0^l \rho(x) * \sum_{i=0}^{4} \phi_i(x)\dot{u}_i\,(t) * \sum_{i=0}^{4} \phi_j(x)\dot{u}_j\,(t) * dx$$

$$= \frac{1}{2}\sum_{i=1}^{4}\sum_{j=1}^{4} \dot{u}_i\,(t)\dot{u}_j\,(t)\int_0^l \rho(x)\phi_i(x)\phi_j(x)dx \tag{3.23}$$

Using Equation (3.23), elemental mass matrix can be evaluated as given in Equation (3.24),

$$\boldsymbol{M^e} = \int_0^l \rho(x)\phi_i(x)\phi_j(x)dx$$

$$= \frac{\rho l}{420}\begin{bmatrix} 156 & 22l & 54 & -13l \\ 22l & 4l^2 & 13l & -3l^2 \\ 54 & 13l & 156 & -22l \\ -13l & -3l^2 & -22l & 4l^2 \end{bmatrix} \tag{3.24}$$

On the other hand, elemental potential energy can be formulated as the Equation (3.25),

$$K = \frac{1}{2}\int_0^l EI(x)[y''(x,t)]^2 dx \tag{3.25}$$

Equation (3.25) can be approximated as Equation (3.26),

$$K = \frac{1}{2}\int_0^l EI(x) * \sum_{i=0}^{4} \phi''_i(x)u_i\,(t) * \sum_{i=0}^{4} \phi''_j(x)u_j\,(t) * dx$$

$$= \frac{1}{2}\sum_{i=1}^{4}\sum_{j=1}^{4} u_i\,(t)u_j\,(t)\int_0^l EI(x)\phi''_i(x)\phi''_j(x)dx \tag{3.26}$$

By using Equation (3.26), elemental stiffness matrix can be computed as given in Equation (3.27),

$$\boldsymbol{K^e} = \int_0^l EI(x)\phi''_i(x)\phi''_j(x)dx$$

$$= \frac{EI}{l^3}\begin{bmatrix} 12 & 6l & -12 & 6l \\ 6l & 4l^2 & -6l & 2l^2 \\ -12 & -6l & 12 & -6l \\ 6l & 2l^2 & -6l & 4l^2 \end{bmatrix} \tag{3.27}$$

Fundamental level results are further extended by the amalgamation of singular elements for the structure as a whole. The effective modeling of the whole structure by assimilating the restraint of geometric compatibility at every element node, i.e. nodal displacements – translations and rotations, pooled by several elements should be alike in nature. The applied forces must be statically similar to the nodal forces – forces and torques. The common set of local displacement coordinates is considered as generalized coordinates of the whole structure. With the help of a fixed-free beam of length L, which is truncated into n elements, has been illustrated in support of complete assembly procedure as shown in figure. For the complete structure, the global displacement vector can be expressed as Equation (3.28),

$$\boldsymbol{u^{g*}} = [\, u_1 \; u_2 \; \ldots\ldots\ldots \; u_{2n+2} \,]^T \tag{3.28}$$

With the consideration of continuity of nodal displacements, global stiffness matrix, $\boldsymbol{K^{g*}}$ can be represented as the Equation (3.29),

$$\boldsymbol{K^{g*}} = \frac{EI}{l^3}\begin{bmatrix} \boldsymbol{K_{11}} & \boldsymbol{K_{12}} & \boldsymbol{0} & \boldsymbol{0} & & \boldsymbol{0} & \boldsymbol{0} \\ \boldsymbol{K_{12}^T} & \boldsymbol{K_{22}} & \boldsymbol{K_{12}} & \boldsymbol{0} & \cdots & \boldsymbol{0} & \boldsymbol{0} \\ \boldsymbol{0} & \boldsymbol{K_{12}^T} & \boldsymbol{K_{22}} & \boldsymbol{K_{12}} & & \boldsymbol{0} & \boldsymbol{0} \\ & & \vdots & & \ddots & \vdots & \\ & \boldsymbol{0} \;\; \boldsymbol{0} & \boldsymbol{0} & \boldsymbol{0} & & \boldsymbol{K_{22}} & \boldsymbol{K_{12}} \\ & \boldsymbol{0} \;\; \boldsymbol{0} & \boldsymbol{0} & \boldsymbol{0} & \cdots & \boldsymbol{K_{12}^T} & \boldsymbol{K_{33}} \end{bmatrix} \tag{3.29}$$

$$\boldsymbol{K_{11}} = \begin{bmatrix} 12 & 6l \\ 6l & 4l^2 \end{bmatrix}, \qquad \boldsymbol{K_{12}} = \begin{bmatrix} -12 & 6l \\ -6l & 2l^2 \end{bmatrix}$$

where,

$$\boldsymbol{K_{22}} = \begin{bmatrix} 24 & 0 \\ 0 & 8l^2 \end{bmatrix}, \qquad \boldsymbol{K_{33}} = \begin{bmatrix} 12 & -6l \\ -6l & 4l^2 \end{bmatrix} \tag{3.30}$$

Similarly, global mass matrix, $\boldsymbol{M^{g*}}$ can be represented as the Equation (3.31),

$$\boldsymbol{M^{g*}} = \frac{\rho}{420}\begin{bmatrix} \boldsymbol{M_{11}} & \boldsymbol{M_{12}} & \boldsymbol{0} & \boldsymbol{0} & & \boldsymbol{0} & \boldsymbol{0} \\ \boldsymbol{M_{12}^T} & \boldsymbol{M_{22}} & \boldsymbol{M_{12}} & \boldsymbol{0} & \cdots & \boldsymbol{0} & \boldsymbol{0} \\ \boldsymbol{0} & \boldsymbol{M_{12}^T} & \boldsymbol{M_{22}} & \boldsymbol{M_{12}} & & \boldsymbol{0} & \boldsymbol{0} \\ & & \vdots & & \ddots & \vdots & \\ & \boldsymbol{0} \;\; \boldsymbol{0} & \boldsymbol{0} & \boldsymbol{0} & & \boldsymbol{M_{22}} & \boldsymbol{M_{12}} \\ & \boldsymbol{0} \;\; \boldsymbol{0} & \boldsymbol{0} & \boldsymbol{0} & \cdots & \boldsymbol{M_{12}^T} & \boldsymbol{M_{33}} \end{bmatrix} \tag{3.31}$$

$$\boldsymbol{M_{11}} = \begin{bmatrix} 156 & 22l \\ 22l & 4l^2 \end{bmatrix}, \qquad \boldsymbol{M_{12}} = \begin{bmatrix} 54 & -13l \\ 13l & -3l^2 \end{bmatrix}$$

where,

$$\boldsymbol{M_{22}} = \begin{bmatrix} 312 & 0 \\ 0 & 8l^2 \end{bmatrix}, \qquad \boldsymbol{M_{33}} = \begin{bmatrix} 156 & -22l \\ -22l & 4l^2 \end{bmatrix} \tag{3.32}$$

By eliminating the first two rows and columns of global mass and stiffness matrices, above boundary conditions are employed. Moreover, in addition of this, the assumption regarding force distribution on the beam is set to be zero. For the complete structure, the improved global displacement vector having size of $2n \times 1$, can be expressed as the Equation (3.33),

$$\boldsymbol{u^g} = [\, u_3 \; u_4 \; \dots \dots \dots \; u_{2n+2} \,]^T \tag{3.33}$$

By considering the boundary conditions (3.18) and canceling the first two row and column stiffness matrix, $\boldsymbol{K^g}$ can be represented as the Equation (3.34),

$$\boldsymbol{K^g} = \frac{\boldsymbol{EI}}{\boldsymbol{l^3}} \begin{bmatrix} \boldsymbol{K_{22}} & \boldsymbol{K_{12}} & \boldsymbol{0} & \boldsymbol{0} & & \boldsymbol{0} & \boldsymbol{0} \\ \boldsymbol{K_{12}^T} & \boldsymbol{K_{22}} & \boldsymbol{K_{12}} & \boldsymbol{0} & \cdots & \boldsymbol{0} & \boldsymbol{0} \\ \boldsymbol{0} & \boldsymbol{K_{12}^T} & \boldsymbol{K_{22}} & \boldsymbol{K_{12}} & & \boldsymbol{0} & \boldsymbol{0} \\ & & \vdots & & \ddots & \vdots & \\ & \boldsymbol{0} \;\; \boldsymbol{0} & \boldsymbol{0} & \boldsymbol{0} & & \boldsymbol{K_{22}} & \boldsymbol{K_{12}} \\ & \boldsymbol{0} \;\; \boldsymbol{0} & \boldsymbol{0} & \boldsymbol{0} & \cdots & \boldsymbol{K_{12}^T} & \boldsymbol{K_{33}} \end{bmatrix} \tag{3.34}$$

$$\boldsymbol{K_{12}} = \begin{bmatrix} -12 & 6l \\ -6l & 2l^2 \end{bmatrix}$$

where,

$$\boldsymbol{K_{22}} = \begin{bmatrix} 24 & 0 \\ 0 & 8l^2 \end{bmatrix}, \qquad \boldsymbol{K_{33}} = \begin{bmatrix} 12 & -6l \\ -6l & 4l^2 \end{bmatrix} \tag{3.35}$$

Similarly global mass matrix, $\boldsymbol{M^g}$ can be represented as the Equation (3.36),

$$\boldsymbol{M^g} = \frac{\rho}{420} \begin{bmatrix} \boldsymbol{M_{11}} & \boldsymbol{M_{12}} & \boldsymbol{0} & \boldsymbol{0} & & \boldsymbol{0} & \boldsymbol{0} \\ \boldsymbol{M_{12}^T} & \boldsymbol{M_{22}} & \boldsymbol{M_{12}} & \boldsymbol{0} & \cdots & \boldsymbol{0} & \boldsymbol{0} \\ \boldsymbol{0} & \boldsymbol{M_{12}^T} & \boldsymbol{M_{22}} & \boldsymbol{M_{12}} & & \boldsymbol{0} & \boldsymbol{0} \\ & & \vdots & & \ddots & \vdots & \\ & \boldsymbol{0} \;\; \boldsymbol{0} & \boldsymbol{0} & \boldsymbol{0} & & \boldsymbol{M_{22}} & \boldsymbol{M_{12}} \\ & \boldsymbol{0} \;\; \boldsymbol{0} & \boldsymbol{0} & \boldsymbol{0} & \cdots & \boldsymbol{M_{12}^T} & \boldsymbol{M_{33}} \end{bmatrix} \tag{3.36}$$

$$\boldsymbol{M_{12}} = \begin{bmatrix} 54 & -13l \\ 13l & -3l^2 \end{bmatrix}$$

where,

$$\boldsymbol{M_{22}} = \begin{bmatrix} 312 & 0 \\ 0 & 8l^2 \end{bmatrix}, \qquad \boldsymbol{M_{33}} = \begin{bmatrix} 156 & -22l \\ -22l & 4l^2 \end{bmatrix} \tag{3.37}$$

3.3.2. Dynamics Modeling of Single-Link Flexible Manipulator using FEM

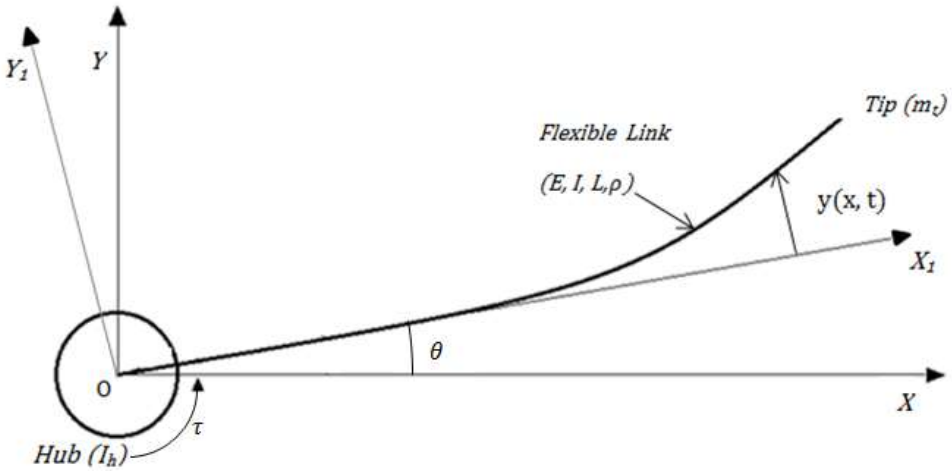

Figure 3.3: Schematic diagram of flexible link

Lagrange approach is utilized and FEM approach is used for the discretization. Each link is thought to be composed of a finite number of elements having equal length. The elements are rigid in compression. However, these considerations are not carried out in the case of bending. Both structural damping and Actuator dynamics is ignored here. The schematic diagram flexible manipulator is shown in Figure 3.3 where OXY and $O_1X_1Y_1$ represent the inertial and body-fixed coordinate frame attached to link respectively, where r is the position vector of a point on the manipulator w.r.t. inertial (OXY) frame; θ is the angular displacement of hub; L , I and ρ are total length, moment of inertia and mass density (mass/length) of *i*ts link respectively; E is Young's modulus; n is the number of elements of link, the elemental kinetic energy i.e. T_j for the j^{th} element of the link is given by Equation (3.38),

$$T_j = \frac{1}{2}\int_0^l \rho \left[\frac{\partial \mathrm{r}}{\partial \mathrm{t}}\right]^{\mathrm{T}} \frac{\partial \mathrm{r}}{\partial \mathrm{t}} \mathrm{dx_j} \tag{3.38}$$

r can be written in term of r_1 w.r.t. to frame $O_1X_1Y_1$

$$\boldsymbol{r} = \boldsymbol{T_0^1 r_1} \tag{3.49}$$

where, $$\boldsymbol{r_1} = \begin{bmatrix} \boldsymbol{(j-1)l + x_j} \\ \boldsymbol{y_j} \end{bmatrix}$$

$$\boldsymbol{T_0^1} = \begin{bmatrix} \cos\theta & -\sin\theta \\ \sin\theta & \cos\theta \end{bmatrix} \tag{3.40}$$

The displacement y_j can be expressed in forms of shape functions $\phi_k(x)$ and nodal displacements $u(t)$, which is given in Equation (3.41),

$$y_j(x_j, t) = \sum_{i=0}^{4} \phi_k(x_j) u_{2j-2+k}(t) \tag{3.41}$$

Using Equation (3.33) and (3.36) element kinetic energy can be obtained as given in Equation (3.42),

$$T_j = \frac{1}{2}\int_0^{\mathrm{l}} \rho \left[\frac{\partial \mathrm{r}}{\partial \mathrm{t}}\right]^{\mathrm{T}} \frac{\partial \mathrm{r}}{\partial \mathrm{t}} \mathrm{dx_j} = \frac{1}{2} \dot{z}^T M \dot{z} \tag{3.42}$$

where, $\boldsymbol{z} = [\ \theta \quad u_{2j-1} \quad u_{2j} \quad u_{2j+1} \quad u_{2j+2}\ ]^T$

$$\boldsymbol{M_j} = \frac{1}{2}\int_0^{\mathrm{l}} \rho \left[\frac{\partial \mathrm{r}}{\partial \mathrm{z_j}}\right]^{\mathrm{T}} \frac{\partial \mathrm{r}}{\partial \mathrm{z_j}} \mathrm{dx_j} \tag{3.43}$$

As z_j contains 5 elements, so M_j will be a 5 × 5 matrix as represented in Equation (3.44),

$$\boldsymbol{M_j} = \begin{bmatrix} m_j(1,1) & m_j(1,2) & m_j(1,3) & m_j(1,4) & m_j(1,5) \\ m_j(1,2) & & & & \\ m_j(1,3) & & \boldsymbol{P_j} & & \\ m_j(1,4) & & & & \\ m_j(1,5) & & & & \end{bmatrix} \tag{3.44}$$

where,

$$m_j(1,1) = \frac{\rho l^3}{3}(3j^2 - 3j + 1) + \boldsymbol{\psi_j^T M_j \psi_j}$$

$$m_j(1,2) = \frac{\rho l^2}{20}(10j - 7)$$

$$m_j(1,3) = \frac{\rho l^2}{60}(5j - 3)$$

$$m_j(1,4) = \frac{\rho l^2}{20}(10j - 3)$$

$$m_j(1,5) = -\frac{\rho l^2}{60}(5j - 2)$$

(3.45)

and $\boldsymbol{P_j} = \mathbf{M}^{\boldsymbol{e}}$ (3.46)

$$\boldsymbol{\psi_j} = [u_{2j-1}\ \ u_{2j}\ \ u_{2j+1}\ \ u_{2j+2}\ ]^T \tag{3.47}$$

In the expression (3.45), $\boldsymbol{P_j}$ denotes the elemental mass matrix of the beam.

Similarly, total element kinetic energy given by Equation (3.48),

$$\bar{T} = \sum_{j=1}^{n} T_j = \frac{1}{2}\dot{\bar{\boldsymbol{q}}}_{\boldsymbol{j}}^{\boldsymbol{T}}\boldsymbol{M_j}\dot{\bar{\boldsymbol{q}}} \tag{3.48}$$

where, $\bar{\boldsymbol{q}} = [\ \theta\ \ \bar{\psi}^T]^T$

$$\bar{\boldsymbol{\psi}} = [u_1\ \ u_2\ \ u_3\ \ \dots\dots u_{2n+2}\ ]^T \tag{3.49}$$

$$\bar{\boldsymbol{M}} = \begin{bmatrix} \bar{m}(1,1) & \bar{m}(1,2) & \bar{m}(1,3) & \dots & \bar{m}(1,2n+3) \\ \bar{m}(1,2) & & & & \\ \bar{m}(1,3) & & & & \\ \vdots & & \bar{\boldsymbol{P}} & & \\ \bar{m}(1,2n+3) & & & & \end{bmatrix} \tag{3.50}$$

where, $\bar{m}(1,1) = \dfrac{\rho l^3 n^3}{3} + \bar{\boldsymbol{\psi}}^{\boldsymbol{T}}\bar{\boldsymbol{P}}\bar{\boldsymbol{\psi}}$

$$\bar{m}(1,2) = \frac{3\rho l^2}{20}$$

$$\bar{m}(1,3) = \frac{\rho l^2}{30}$$

$$\bar{m}(1,4) = \rho l^2$$

$$\bar{m}(1,5) = \frac{\rho l^2}{15}$$

$$\bar{m}(1,2\mathrm{k}) = (\mathrm{k}-1)\rho l^2 \qquad \forall\ k = 2,3,\dots\dots,n$$

$$\bar{m}(1,2\mathrm{k}+1) = \frac{\rho l^2}{15} \qquad \forall\, k = 2,3,\ldots\ldots,n$$

$$\bar{m}(1,2\mathrm{n}+2) = \frac{\rho l^2}{20}(10n-3)$$

$$\bar{m}(1,2\mathrm{n}+3) = -\frac{\rho l^2}{60}(5n-2) \tag{3.51}$$

And $$\bar{\mathbf{P}} = \mathbf{M}^{g*} \tag{3.52}$$

In the Equation (3.52), $\bar{\boldsymbol{P}}$ denotes the expression of global mass matrix of the beam.

After, applying boundary condition i.e. $u_1 = u_2 = 0$ deleting the second and third column and row we get mass matrix of a flexible link as represent by Equation (3.55),

$$T = \frac{1}{2}\boldsymbol{q}_j^{\cdot T}\boldsymbol{M}_j\boldsymbol{q}^{\cdot} \tag{3.53}$$

where, $$\boldsymbol{q} = [\,\theta \;\; \boldsymbol{\psi^t}]^T$$

$$\boldsymbol{\psi} = [u_3 \;\; u_4 \;\; u_5 \;\ldots\ldots u_{2n+2}\,]^T \tag{3.54}$$

$$\boldsymbol{M} = \begin{bmatrix} m(1,1) & m(1,2) & m(1,3) & \ldots & m(1,2n+1) \\ m(1,2) & & & & \\ m(1,3) & & & & \\ \vdots & & \boldsymbol{P} & & \\ m(1,2n+1) & & & & \end{bmatrix} \tag{3.55}$$

where,

$$m(1,1) = \frac{\rho l^3 n^3}{3} + \boldsymbol{\psi^T P \psi}$$

$$m(1,2\mathrm{k}-2) = (\mathrm{k}-1)\rho l^2 \qquad \forall\, k = 2,3,\ldots\ldots,n$$

$$m(1,2\mathrm{k}-1) = \frac{\rho l^2}{15} \qquad \forall\, k = 2,3,\ldots\ldots,n$$

$$m(1,2\mathrm{n}) = \frac{\rho l^2}{20}(10n - 3)$$

$$m(1,2\mathrm{n}+1) = -\frac{\rho l^2}{60}(5n - 2) \tag{3.56}$$

And $$\mathbf{P} = \mathbf{M}^{\boldsymbol{g}} \tag{3.57}$$

In the above expression of Equation (3.55), $\boldsymbol{P}$ signifies the global mass matrix of the beam.

Similarly, the total potential energy of the link can be calculated as given in Equation (3.58),

$$P.E. = P.E._g + P.E._e \tag{3.58}$$

where, $P.E._g$ is gravitational potential energy

$P.E._e$ is element potential energy

$$P.E. = \rho g[0 \quad 1]\boldsymbol{T_0^1}\begin{bmatrix}\frac{nl^2}{2}\\ \boldsymbol{R\psi}\end{bmatrix} + \frac{1}{2}\boldsymbol{\psi^T K_s \psi} \tag{3.59}$$

$$\boldsymbol{R} = \left[|l \quad 0| \quad |l \quad 0| \quad |l \quad 0||l \quad 0| \quad |\cdots \quad \cdots| \quad \left|\frac{l}{2} \quad -\frac{l^2}{12}\right|\right] \quad \forall\, i = 1,2 \tag{3.60}$$

$$\boldsymbol{K_s} = \boldsymbol{K^g} \tag{3.61}$$

In the above expression, $\boldsymbol{K_s}$ is calculated by using Equation (3.34).

Lagrangian, $\mathcal{L}$ of the system is given by subtraction of total kinetic energy and total potential energy of the system, given as:

$$\mathcal{L} = K.E. - P.E. \tag{3.62}$$

Heat or damping losses due to friction at shaft of rotation is given by Equation (3.63),

$$H = \frac{1}{2}\dot{\theta} D_b \dot{\theta} \tag{3.63}$$

Using Lagrange Equations (3.6), the dynamic model of the two-link flexible manipulator can be written as the Equation (3.69),

with $$\frac{\partial \mathcal{L}}{\partial \boldsymbol{q}^{\cdot}} = \boldsymbol{M}\boldsymbol{q}^{\cdot} \tag{3.65}$$

$$\frac{\partial \mathcal{L}}{\partial \theta} = -\rho g[0\ 1]\boldsymbol{T_0^1}\begin{bmatrix}\frac{1}{2}n^2l^2 \\ \boldsymbol{R\psi}\end{bmatrix} \tag{3.66}$$

$$\frac{\partial \mathcal{L}}{\partial \boldsymbol{\psi}} = \theta^{\cdot 2}\boldsymbol{P\psi} - \rho g[0\ \boldsymbol{R}]\boldsymbol{T_0^1}^T\begin{bmatrix}0\\1\end{bmatrix} - \boldsymbol{K_s\psi} \tag{3.67}$$

$$\frac{\partial H}{\partial \theta^{\cdot}} = D_b\theta^{\cdot} \tag{3.68}$$

Dynamics of the flexible manipulator is given by Equation (3.69)

$$\boldsymbol{M(q)q}^{\cdot\cdot} + \boldsymbol{n(q,\dot{q})} = \boldsymbol{\tau} \tag{3.69}$$

where, $\boldsymbol{q} = [\theta \quad \boldsymbol{\psi^T}]^T$, is generalized displacement vector (3.70)

$\boldsymbol{\tau} = [\tau \quad f_{1,3} \quad f_{1,4} \ \ldots\ldots f_{1,2n+3}]$, is generalized force vector (3.71)

$$\boldsymbol{M(q)} = \boldsymbol{R^{(2n+1)\times(2n+1)}} \tag{3.72}$$

,is symmetric positive-definite inertia matrix

$$\mathbf{n}(\mathbf{q},\dot{\mathbf{q}}) = -\left[\frac{\partial \mathcal{L}}{\partial \theta} + \frac{\partial H}{\partial \theta^{\cdot}}, \frac{\partial \mathcal{L}}{\partial u_3}, \ldots, \frac{\partial \mathcal{L}}{u_{2n}}, \frac{\partial \mathcal{L}}{u_{2n+1}}\right]^T \tag{3.73}$$

,is vector of Coriolis, centripetal, gravitational and elastic forces

Obtained dynamics of the flexible manipulator is in the form of the non-linear Equation. Linearize Equation of motion about the stable point of flexible manipulator i.e. for any value of θ and $\psi = 0$ is given by Equation (3.74)

$$\boldsymbol{M_l\ddot{q} + N_l\dot{q} + G_lq} = \boldsymbol{\tau} \tag{3.74}$$

By writing state vector as $\boldsymbol{x(t) = [q^T, q^{\cdot T}]^T}$ the state space representation of flexible manipulator is given by Equation (3.75),

$$\boldsymbol{\dot{x}(t) = A_{fem}x(t) + B_{fem}u(t)} \tag{3.75}$$

where, $\boldsymbol{A_{fem} = \begin{bmatrix} 0_n & I_n \\ -M_L^{-1}G_L & -M_L^{-1}N_L \end{bmatrix}}$ and $\boldsymbol{B_{fem} = \begin{bmatrix} 0_n \\ M_L^{-1} \end{bmatrix}}$ (3.76)

3.4. Augmentation of the Actuator Dynamics

Both finite element model and lumped parameter model are, derived for torque, applied at the hub of the flexible manipulator. Torque is generated by the DC motor when voltage (V_m) is applied and given in Equation (3.77).

$$\tau = \frac{\eta_g K_g \eta_m K_t (V_m - K_g K_m \dot{\theta})}{R_m} \tag{3.77}$$

where, η_g is gear box efficiency, K_g is reduction ratio of motor shaft to load shaft, η_m is motor efficiency, R_m is armature resistance, K_m is motor torque constant.

Adding motor dynamics in state-space model, modified element of state-space is represented Equation (3.78) and (3.79)

$$\boldsymbol{A_m}\left(\frac{n_0}{2}:n_0,\frac{n_0}{2}\right) = \boldsymbol{A}\left(\frac{n_0}{2}:n_0,\frac{n_0}{2}\right) - \boldsymbol{B}\left(\frac{n_0}{2}:n_0\right) * \eta_g * K_g * \eta_m * k_t * k_m/R_m; \tag{3.78}$$

$$\boldsymbol{B_m} = \eta_g K_g \eta_m \frac{k_t}{R_m}\boldsymbol{B}; \tag{3.79}$$

where, n_0 is size of the generalized state vector,

3.5. Summary

This chapter has presented two mathematical models of flexible manipulator system. All mathematical calculation for obtaining the dynamics of the flexible manipulator is performed in MATLAB R2016a environment. In Chapter 4, these models are used for checking the controllability of the model and designing the controller parameters to achieve better performance of a flexible manipulator in control theory. The description of corresponding SRV02 parameters are discussed in Chapter 5. These parameters are utilized to evaluate

mathematical models as per discussions of this chapter and the actuator dynamics is augmented with the flexible manipulator's mathematical model. These two models are compared with a real-time model in Chapter 6. Effect of changing the dimensions of link and payload on natural frequency is also examined in Chapter 6 by using finite element model.

Chapter 4

Control of Flexible Manipulators

4.1. Introduction

In this chapter, controller design is discussed for a single-link flexible manipulator. In flexible-link manipulator, the major problem is to control the tip deflection to achieve any position of shaft angle (θ), which is being addressed in this thesis work. There are several controllers available to address the deflection problem of flexible manipulator. The aim of this chapter is to design two controllers by using the state-space representation derived by lumped parameter method, as discussed in Chapter 3. Linearized mathematical model is utilized to design the controllers, thus there is need to develop robust controller for the problem. The prime objective of the controller is to minimize the tip deflection while tracking the shaft angle and second objective is to achieve robustness to model uncertainty as well as input disturbance. To achieve these objectives, two controllers are discussed in this chapter. As discussed in Chapter 2, selection of the weight matrices to achieve desire performance of system with LQR controller is a time-consuming job. Further, Genetic algorithms are proposed for the optimization of weight matrices. Before implementing the controllers, first step is to check the controllability of the system.

4.2. Controllability of the System

To control any system in the world, first and the foremost requirement is to ensure the controllability of the system. Controllability is defined as the property of a system when it is possible to take the system from any initial state to any final state in a finite time by means of the input vector. Controllability of any system can be checked easily from the state-space representation of the system.

The theorem for controllability state that, "*A linear, time-invariant system described by the matrix state-equation,* $\dot{\boldsymbol{x}} = \boldsymbol{Ax} + \boldsymbol{Bu}$ *is controllable if and only if the controllability test matrix is of rank n, the order of the system*". The controllability of the system can also be checked from in-built MATLAB function $ctrb(\boldsymbol{A}, \boldsymbol{B})$, which is based on the above theorem. The controllability test Matrix is represented by Equation (4.1),

$$\boldsymbol{C_f = [B; AB;\ A^2B; \ldots\ldots\ldots\ldots\ldots, A^{n-1}B]} \tag{4.1}$$

4.3. Linear Quadratic Regulator (LQR) Control

Linear Quadratic Regulator (LQR) is an optimal control technique, which is used to minimize the cost associated with generating control inputs. The cost function consists of two matrices, Q and R, i.e. state weighting matrix and control cost matrix respectively. LQR addresses the desired performance of system directly, provided one must know precisely how to translate the objective into the cost function. For a linearized plant, the objective of LQR controller is to minimize the integration of sum of these two matrices from initial to final time by using a feedback regulator. Schematic flow diagram of LQR is as shown in Figure 4.7. For the flexible manipulator system with u input and x variable vector, the feedback is given as:

$$\boldsymbol{u = K(x_d - x)} \tag{4.2}$$

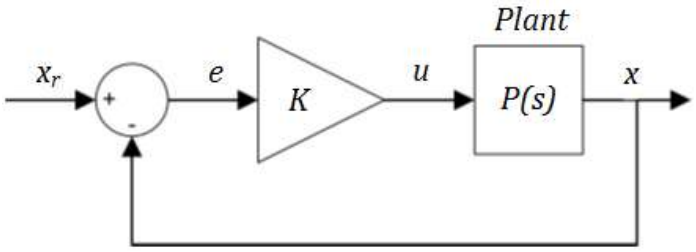

Figure 4.1: Block diagram of LQR

And cost function i.e. the objective is given as:

$$J_o = \int_0^\infty (\boldsymbol{x^T Q x + u^T R u})dt \tag{4.3}$$

Where, K is the final optimal state feedback control matrix, which is given as

$$\boldsymbol{K = R^{-1} B^T P} \tag{4.5}$$

Here, P is the following symmetric positive definite solution of the Equation (4.6)

$$\boldsymbol{PA + A^T P - PBR^{-1}B^T P + Q = 0} \tag{4.6}$$

It can be seen, matrix depends on $\boldsymbol{A}, \boldsymbol{B}, \boldsymbol{Q}$, and $\boldsymbol{R}$ matrix, $\boldsymbol{A}$ and $\boldsymbol{B}$, are determined by the structure and parameters of the system respectively, so really depends on the weight matrix $\boldsymbol{Q}$ and $\boldsymbol{R}$. Select $\boldsymbol{Q}$ and $\boldsymbol{R}$ according to expected performance criterion, the matrix $\boldsymbol{K}$ can be easily obtained by MATLAB command *lqr* as represented by Equation (4.7).

$$\boldsymbol{K} = lqr(\boldsymbol{A}, \boldsymbol{B}, \boldsymbol{Q}, \boldsymbol{R}) \tag{4.7}$$

Change in the weights of $\boldsymbol{Q}$ matrix will results in different system response. Generally, the control weight matrices are taken as $\boldsymbol{R} = \boldsymbol{1}, \boldsymbol{Q} = \boldsymbol{C}' \times \boldsymbol{C}$. The expected response could also be achieved through adjusting the controller by changing nonzero element in matrix $\boldsymbol{Q}$.

For the given single-link flexible manipulator, ,, the state vector is taken as $\boldsymbol{x} = \left[\theta \;\; \alpha \;\; \dot{\theta} \;\; \dot{\alpha}\right]^T$. Since our system has just one control variable, R will be a scalar quantity. The reference signal $\boldsymbol{x_{ref}}$ is set to $[\theta_r \; 0 \; 0 \; 0]^T$, and therefore control input to the system can be written as,

$$\boldsymbol{u} = \boldsymbol{K}(\boldsymbol{x_d} - \boldsymbol{x}) = k_{p,\theta}(\theta_d - \theta) - k_{p,\alpha}\alpha - k_{d,\dot{\theta}}\dot{\theta} - k_{d,\dot{\alpha}}\,\dot{\alpha} \tag{4.8}$$

Selection of Weight Matrices by Genetic Algorithms(GA)

The schematic diagram of the implementation of GA is as shown in Figure 4.2. LQR deals directly with the performance of the system for selected weight matrices. Selection of $\boldsymbol{Q}$ and $\boldsymbol{R}$ to obtain desired system performance is achieved by trial and error methods. However, GA can be utilized as an optimization tool to find out the optimum value of $\boldsymbol{Q}$ and $\boldsymbol{R}$**.** Error of the system to reach steady state is chosen as performance index. Objective fitness functions to optimize $\boldsymbol{Q}$ and $\boldsymbol{R}$ is integral absolute error (integration of sum of absolute error in theta and alpha), is represented by Equation (4.9),

$$IAE = \int_0^T [|e_\theta(t)| + |e_\alpha(t)|]dt \tag{4.9}$$

where, e_θ is error in of shaft angle and e_α is error in tip deflection.

Genetic algorithms are stochastic search techniques that guide a population of solutions towards an optimum value. The set of population of the two variables $\boldsymbol{Q}$ and $\boldsymbol{R}$, selected randomly, is initialized by the GA. All members of population are evaluated by the algorithm according to the specified performance index. The new set of population is generated by using GA operators - *reproduction*, *crossover* and *mutation*, on the basis performance of

members of population. The population's best member is selected foe next generation. Again the best member of this new population is selected by applying GA operations. The new population's best member is compared to previous member's best member. At last, the best member among all is selected.

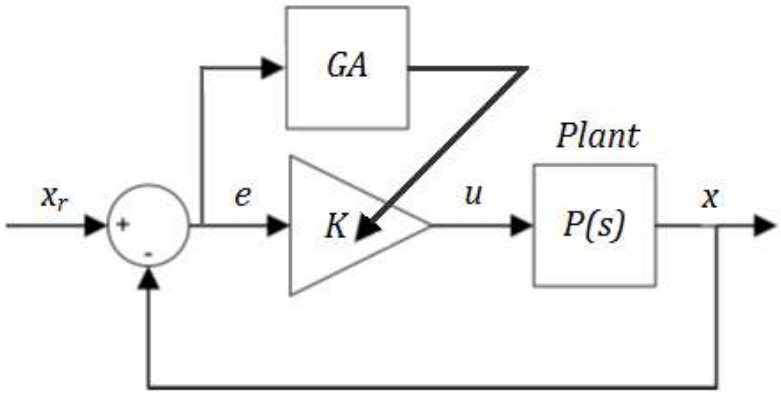

Figure 4.2: Block diagram represent GA based LQR

4.4. Integral Sliding Mode Control (ISMC)

Integral sliding mode ensures the robustness during entire response of the system to model parameter uncertainties and input uncertainties [48],[49]. For a flexible manipulator system, LQR feedback control is already designed. To tackle the problem of model uncertainties and input disturbances, a continuous term is added to the input of LQR system which is based on integral sliding mode. This continuous term ensure the desired performance in presence of input disturbance. Feedback control law of linearized dynamics of the flexible manipulator is given by Equation (4.2). However, this control law is designed for ideal system dynamics of flexible manipulator. Dynamic model with input disturbances is represented by Equation (4.10),

$$\dot{\boldsymbol{x}} = \boldsymbol{Ax} + \boldsymbol{Bu} + \boldsymbol{g}(\boldsymbol{x}, \boldsymbol{t}) \tag{4.10}$$

where, $\boldsymbol{g}(\boldsymbol{x}, \boldsymbol{t})$ is the external disturbance represent by Equation (4.11),

$$\boldsymbol{g}(\boldsymbol{x}, \boldsymbol{t}) = \boldsymbol{B}\boldsymbol{u}_{\boldsymbol{d}} \tag{4.11}$$

Equation (4.11) represents that input disturbance, $\boldsymbol{u}_{\boldsymbol{d}}$ influence all states of the dynamic system via input state matrix $\boldsymbol{B}$. The boundedness of the input disturbance can be ensure with a positive number M_0, which is greater than the maximum magnitude of input disturbance.

$$M_0 > |\boldsymbol{g}(\boldsymbol{x}, \boldsymbol{t})| \tag{4.12}$$

The system control law is illustrated by Equation (4.13),

$$u_s = u + u_0 \tag{4.13}$$

where u_0 is the discontinuous control input which is designed to eliminate the external disturbance.

Sliding surface of the dynamic system is given by Equation (4.14),

$$s(x,t) = \boldsymbol{G}\left[\boldsymbol{x}(\boldsymbol{t}) - \boldsymbol{x}(\boldsymbol{0}) - \int_{\boldsymbol{0}}^{\boldsymbol{t}} (\boldsymbol{Ax} + \boldsymbol{Bu_0})\boldsymbol{d\tau}\right] \tag{4.14}$$

where, u_0 is input from the controller without disturbance. $\boldsymbol{G}$, is the projection matrix. The matrix $\boldsymbol{G}$ must be chosen such that $\boldsymbol{GB}$ is invertible. Therefore, $\boldsymbol{G}$ could be pseudo inverse of $\boldsymbol{B}$: represented by Equation (4.15),

$$\boldsymbol{G} = (\boldsymbol{B^T B})^{-1}\boldsymbol{B^T} \tag{4.15}$$

which leads to,

$$\boldsymbol{GB} = (\boldsymbol{B^T B})^{-1}\boldsymbol{B^T B} = \boldsymbol{I} \tag{4.16}$$

Therefore, Equation (4.16) suggests that the inverse of GB exist.

Control input u_0 is given by Equation (4.17),

$$u_0 = -M_0 sign(s) \tag{4.17}$$

Control law represented by Equation (4.16) will lead to chattering to avoid the same use input as illustrated in Equation (4.18),

$$u_0 = -M_0\left(\frac{s}{|s| + \epsilon}\right) \tag{4.18}$$

Where, ϵ is very small positive value.

4.5. Summary

In this chapter, two controllers are designed that are linear quadratic regulator and integral sliding mode control. Both of these controllers are designed using lumped parameter model of flexible manipulator that is derived in Chapter 3. The comparative analysis of both the models with each other, and with the real-time model is discussed in Chapter 6.

Chapter 5

Experimental Setup

5.1. Introduction

The experimental set-up of single-link flexible manipulator is shown in Figure 5.1, which is developed by Quanser, Ontario, Canada. Experimental setup of flexible link manipulator consists of a flexible link, a drive unit (SRV 02), a data acquisition board and a power amplifier.

Figure 5.1: Quanser flexible manipulator setup.

5.2. Components of the Flexible Manipulator

Various components of the flexible manipulator setup are listed below:

Flexible link: The flexible link shown in Figure 5.2 is a thin stainless steel flexible scale of length L. Strain gauge is mounted on flexible link on the clamp end to detect the tip deflection in the form of a analog signal. The flexible link is mounted on the shaft of SRV 02 (drive unit) to give rotational motion. Material properties and dimensions of the link are given in Table 5.1.

Figure 5.2: Flexible link

These parameters are then put in mathematical model derived in Chapter 3 and controllers are design based on that mathematical model.

Table 5.1: Parameters of the Quanser flexible link [50].

S.No.	Parameter	Units	Symbol	Value
1	Length of link	m	L	0.419
2	Width of link	m	h	20.73×10^{-3}
3	Thickness of link	m	b	0.79×10^{-3}
4	Mass per unit length	kg/m	ρ	.155
5	Area moment of inertia	m^4	I	8.15×10^{-13}
6	Young's modulus	N/m^2	E	170×10^{9}
7	Cross-sectional area	m^2	a	2.15×10^{-5}
8	Stiffness of link (rotational)	Nm/rad	K_s	1.3

Drive unit (SRV02): The Quanser SRV02 plant given in Figure 5.3 consists of DC servo motor (Faulhaber Coreless DC Motor model 2338S006), which is connected with a internal gear box of reduction ratio 1:14. Motor shaft is coupled with the load shaft through gears which further reduce the motion by ratio of 1:5. Combining both gear ratio results in a total reduction of 1:70.

Figure 5.3: Quanser SRV02 drive unit

Load shaft is coupled with an optical encoder offering high resolution of 4096 counts per revolution in quadrature mode (1024 line per revolution). Encoder measures the angular position of the load shaft. Furthermore, angular position of the shaft can also be measured by a continuous potentiometer. Thereafter, a tachometer is coupled with the motor shaft to measure its angular velocity. Specification of motor and other component is given in Table 5.2.

Table 5.2: Parameters of SRV02 [51]

S.No.	Parameter	Units	Symbol	Value
1	Armature resistance	Ohm	R_m	2.6
2	Motor torque constant	Nm/A	k_t	7.67×10^{-3}
3	Hub inertia / Equivalent moment of inertia	Nm^2	I_{hub}	2.087×10^{-3}
4	Damping of load shaft	Nm/(rad/sec)	D_b	.015
5	Gearbox efficiency	-	η_g	0.9
6	Motor efficiency	-	η_m	0.69
7	Transmission Ratio	-	K_g	70

Data acquisition board (Q8-USB): The Q8-USB data acquisition board shown in Figure 5.4. Q8-USB is having wide-range for input and output ports. Eight port each for analog inputs and analog outputs, eight more ports for encoders i.e. digital inputs. It is easy to connect with computer with USB cable.

Figure 5.4: Q8-USB data acquisition board

Amplifier (VoltPAQ-X1): The VoltPAQ-X1 is as shown in Figure 5.5. It can power one load. The amplifier realizes the power adaptation between the data acquisition board and SRV02 the drives the flexible manipulator.

Figure 5.5: Power Amplifier (VoltPAQ-X1)

5.3. Layout of the Flexible Manipulator

Layout representing flow of signal in flexible manipulator setup is illustrated by Figure 5.2. The digital signal from encoder (mounted on rotating shaft) is transferred to data acquisition board and also, analog signal from strain gauge (mounted on flexible link) is transferred to data acquisition board. Reading from both encoders and strain sensor is transfer to the Simulink. Simulink calculates the input for the plant and pass it to data acquisition board. Thereafter, signal from data acquisition board is transfer to the plant through amplifier.

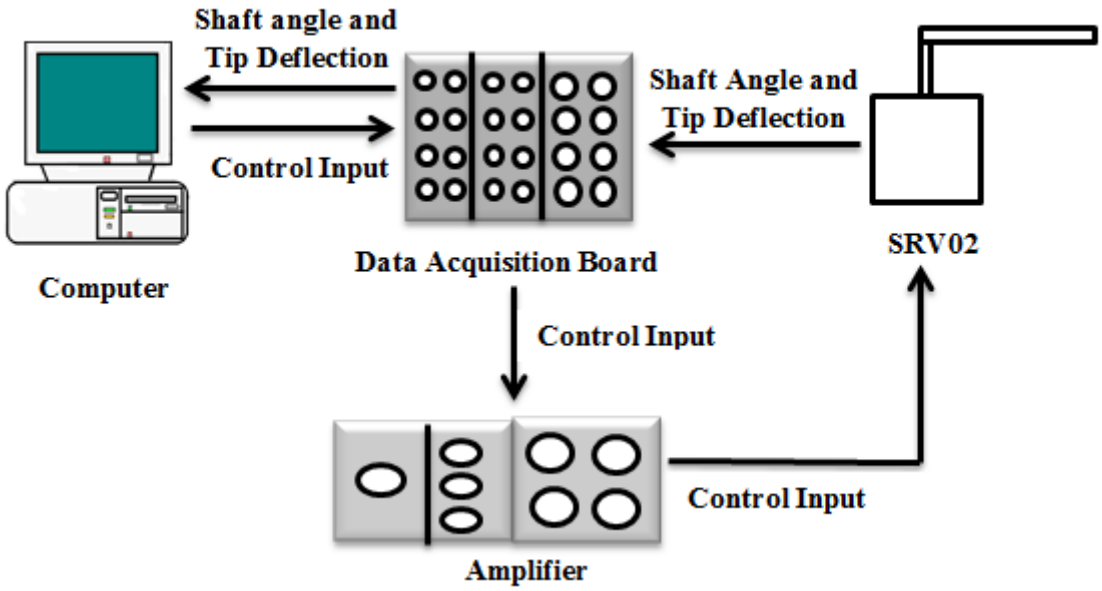

Figure 5.6: Layout represent data flow

5.4. Summary

In this chapter, experimental setup of the single-link flexible manipulator is discussed. Furthermore, list of the components of flexible manipulator and their features are illustrated. Parameters of both derive unit and flexible link are discussed in Table 5.1 and 5.2 respectively, which are to be plugged in while deriving the mathematical model of the system, as discussed in the Chapter 3. The control techniques are illustrated in the Chapter 4 and are implemented on experimental model in the Chapter 6. Finally, comparative analysis of both the models is demonstrated in Chapter 6.

Chapter 6

Results and Discussions

6.1. Introduction

Two ways of solving the dynamics of system are shown in Chapter 3. The prime objective in this chapter is to validate both the models. After validation, variation of the frequency with different parameters of flexible manipulator is discussed. Furthermore, as per discussions in Chapter 4, controllers are implemented and their performance for parametric uncertainty and input disturbance is elaborated. The efficacy of the both LQR and integral sliding mode controllers is checked in simulation as well in real-time environment.

6.2. Experimental Validation

Time-domain validation of both the models in real-time scenario is done by substituting parameters of the plant and motor, as given in Table (5.1) and (5.2). The state-space representation for finite element model is given by Equation (6.1) and for lumped parameter model is illustrated by Equation (6.2).

$$\boldsymbol{A_{fem}} = \begin{bmatrix} 0 & 0 & 0 & 1 & 0 & 0 \\ 0 & 0 & 0 & 0 & 1 & 0 \\ 0 & 0 & 0 & 0 & 0 & 1 \\ 0 & 4880.9 & -1071.3 & -39.384 & 0 & 0 \\ 0 & 5061.9 & -1799.6 & 14.852 & 0 & 0 \\ 0 & 133250 & -40750 & -11.815 & 0 & 0 \end{bmatrix}, \quad \boldsymbol{B_{fem}} = \begin{bmatrix} 0 \\ 0 \\ 0 \\ 60.232 \\ -22.713 \\ 18.070 \end{bmatrix} \tag{6.1}$$

$$\boldsymbol{A_{lum}} = \begin{bmatrix} 0 & 0 & 1 & 0 \\ 0 & 0 & 0 & 1 \\ 0 & 622.90 & -40.177 & 0 \\ 0 & -965.01 & 40.177 & 0 \end{bmatrix}, \quad \boldsymbol{B_{lum}} = \begin{bmatrix} 0 \\ 0 \\ 61.445 \\ -61.445 \end{bmatrix} \tag{6.2}$$

Comparative analysis is illustrated by evaluating the shaft angle and tip deflection, as shown in Figures 6.1 and 6.2, respectively for the given step input to the motor. In Figure 6.1, both mathematical models track the real-time model exactly during the transient phase. However, slight steady-state error is observed among mathematical models and real-time model, which

might occur due to the presence of Coulomb friction or deviation in value of viscous damping, which are not included in the mathematical model.

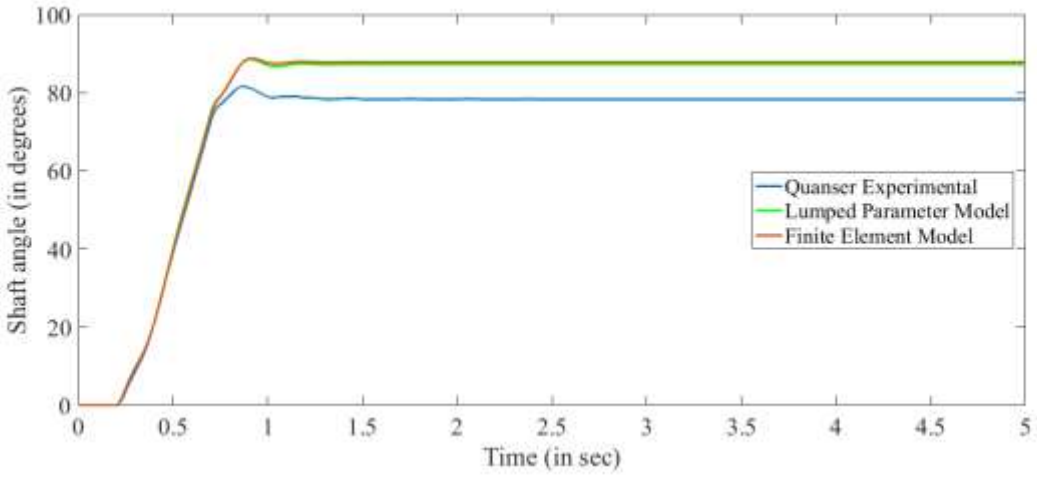

Figure 6.1: Comparative analysis of shaft angle to step response for three models.

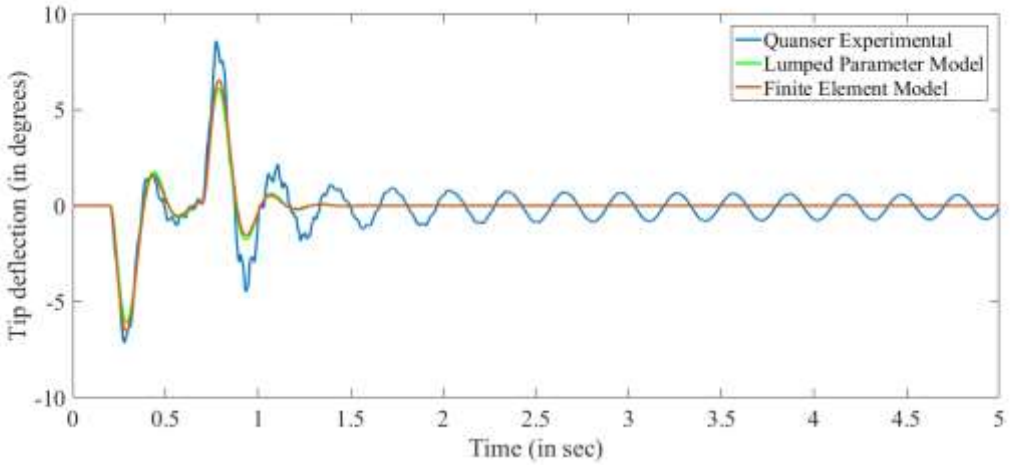

Figure 6.2: Comparative analysis of tip deflection to step response for three models.

In Figure 6.2, finite element model overlaps with real-time model for first few oscillations. However, both models don't show the deflection for latter oscillations having low amplitude. This may happen due to linear mathematical models, where flexible manipulator is highly nonlinear in real practice. It may also occur due to the consideration of less number of elements of the flexible link during the mathematical modeling.

6.3. Frequency Analysis of the Flexible Manipulator

In this section, variation in natural frequency of the single-link flexible manipulator is demonstrated by adjusting different parameters of the system. The adjusting parameters are length of the link (L), flexural rigidity (EI) and mass of the manipulator (m). Initially,

payload and hub inertia is assumed to be zero. Thereafter, the study on the variation of payload (m_t) with frequency is carried out. In Figure 6.3, flexural rigidity of the flexible manipulator is considered within the range of 0-5 Nm^2. It is observed that natural frequency of both the modes increases with increase in flexural rigidity. However, increment in the value of second mode is very high in comparison with first mode. In Figure 6.4, it is illustrated that frequency is decreasing with increase in mass of the flexible manipulator. In Figure 6.5, the variation of frequency with the length of the manipulator, for two different types of materials, is illustrated. The flexural rigidity of the two materials is 0.144 Nm^2 and 0.288 Nm^2, respectively. It is observed that with the increase in length, the frequency decreases. However, for second mode, material having flexural rigidity 0.288 Nm^2 differs significantly as compared to the material with flexural rigidity 0.144 Nm^2. In Figure 6.6, payload is considered within the range 0-100 grams and observed that frequency of first mode is not getting affected, significantly. However, frequency of second mode has changed ominously.

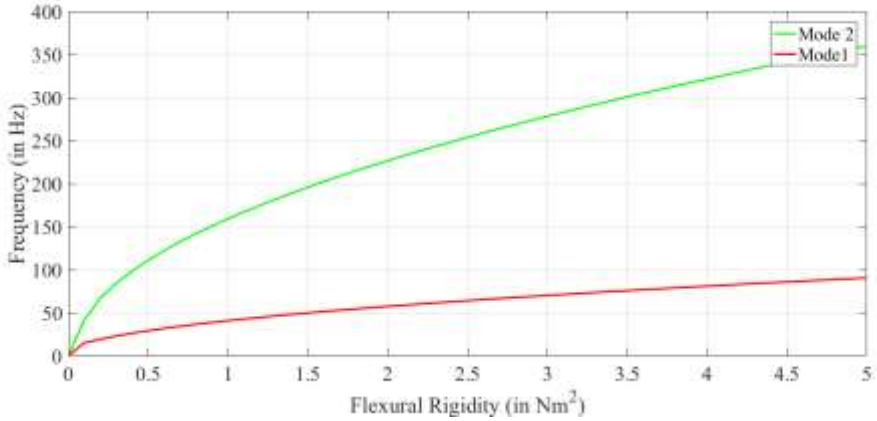

Figure 6.3: Variation of natural frequency with flexural rigidity of flexible link

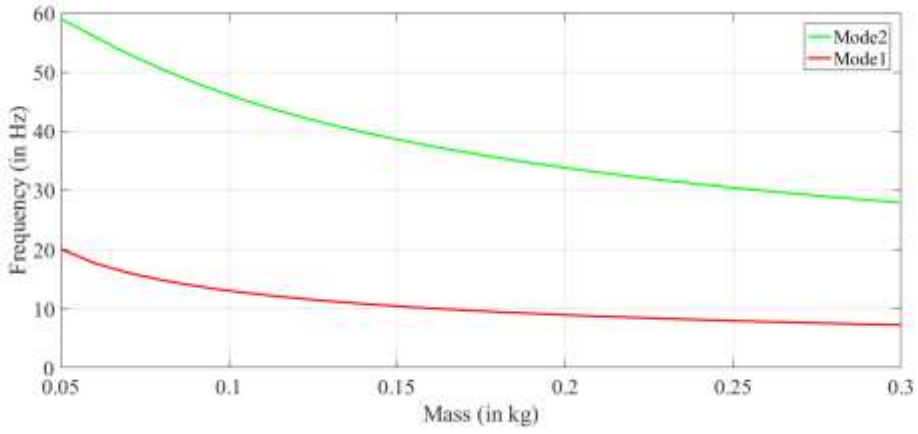

Figure 6.4: Variation of natural frequency with mass of the flexible link

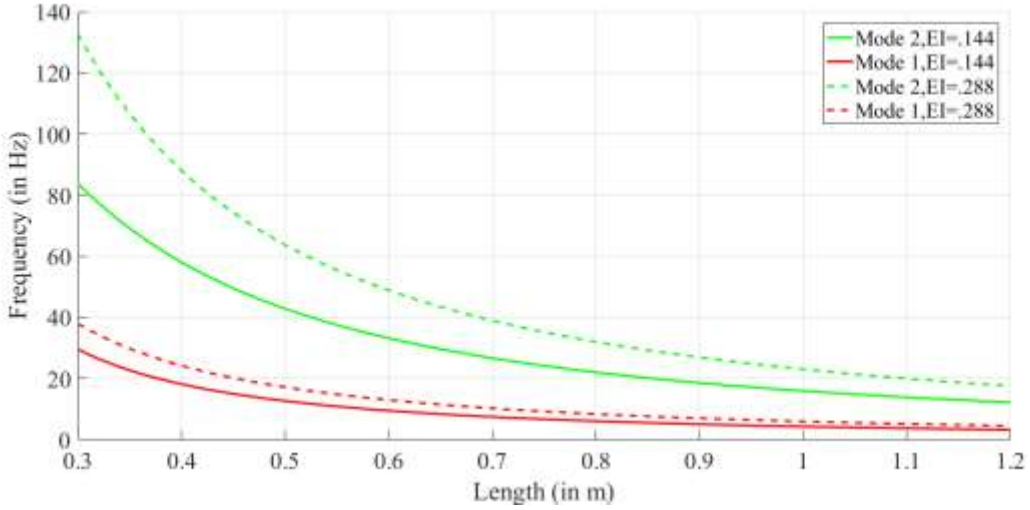

Figure 6.5: Variation of natural frequency with length of the flexible link

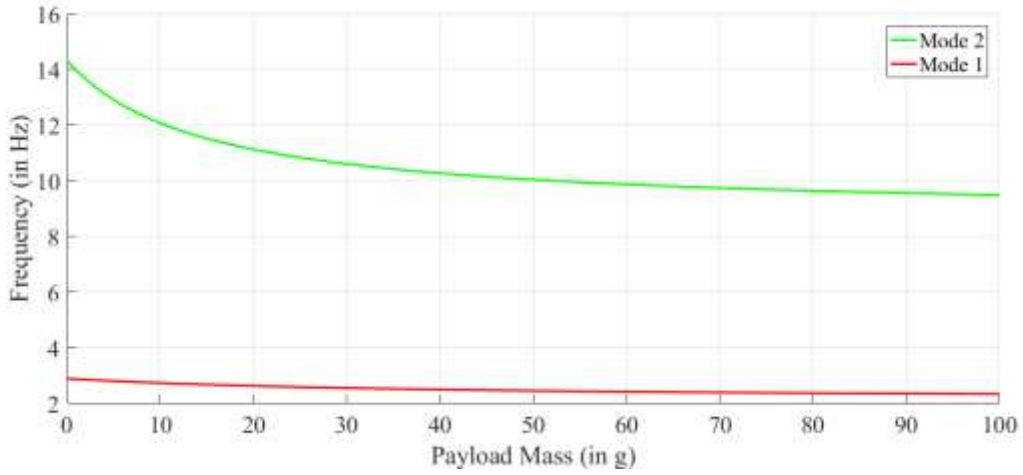

Figure 6.6: Variation of natural frequency with payload on flexible link

6.4. LQR Controller Without Input Disturbance

Controllability of the lumped system, given in Equation (6.2) is analysed. With the checking of controllability of the system it is found that controllability matrix ($\boldsymbol{C_f}$) is given by Equation 6.3, having the rank of 4. This ensures that the system is controllable.

$$\boldsymbol{C_f} = \begin{bmatrix} 0 & 61.44 & -2468.70 & -60912.00 \\ 0 & -61.44 & 2468.70 & 39891.00 \\ 61.44 & -2468.70 & 60912.00 & -909510.00 \\ -61.44 & 2468.70 & -39891.00 & 64948.00 \end{bmatrix} \tag{6.3}$$

In Figure 6.6, the Simulink diagram of flexible link manipulator with LQR control is illustrated. State-space used Simulink model is of lumped parameter model is given by Equation (6.2).

Three cases for weight matrices $\boldsymbol{Q}$ and $\boldsymbol{R}$ are considered for testing and validation of the concerned problem. In the first two cases, the values of weight matrices are not optimized whereas in the last case, optimization of weight matrices is carried out with the help of Genetic Algorithms. In Table 6.1, the comparative analysis of above three cases is tabulated.

Table 6.1: Value of Q, R and K three different cases

	State Weight Matrix, $\boldsymbol{Q}$	**Input Weight Matrix, $\boldsymbol{R}$**	**Gain $\boldsymbol{K}$**
Case 1 (Hit and trial)	$\begin{bmatrix} 150 & 0 & 0 & 0 \\ 0 & 1 & 0 & 0 \\ 0 & 0 & 1 & 0 \\ 0 & 0 & 0 & 3 \end{bmatrix}$	[1]	$\begin{bmatrix} 12.25 \\ -22.79 \\ 1.33 \\ -0.37 \end{bmatrix}^T$
Case 2 (Hit and trial)	$\begin{bmatrix} 125 & 0 & 0 & 0 \\ 0 & 1 & 0 & 0 \\ 0 & 0 & 1 & 0 \\ 0 & 0 & 0 & 3 \end{bmatrix}$	[1]	$\begin{bmatrix} 11.18 \\ -22.79 \\ 1.33 \\ -0.37 \end{bmatrix}^T$
Case 3 (optimize by GA)	$\begin{bmatrix} 136.52 & 0 & 0 & 0 \\ 0 & 40.53 & 0 & 0 \\ 0 & 0 & 1.3 & 0 \\ 0 & 0 & 0 & 0.56 \end{bmatrix}$	[5]	$\begin{bmatrix} 5.22 \\ -10.3 \\ 0.56 \\ -0.25 \end{bmatrix}^T$

In Figure 6.6, comparative analysis of three case studies with the desired trajectory for shaft angle is presented. The reference trajectory denotes shaft angle is considered as a square wave having frequency as 2 rad/sec and amplitude of 30 degrees. The first two cases almost behave in a similar fashion with the overshoot of 2.8% and 1.8% respectively. However, the third case having optimized weight matrices from GA behave distinctly with no overshoot. The settling time for all the three cases is approximately of the same order with the values as0.42 sec, 0.46 sec and 0.43 sec, respectively.

In Figure 6.7, comparative analysis with the same case studies for tip deflection is illustrated. The tip deflection should be as minimum as possible. It is inferred from the figure that first two cases approximately behave in similar manner with high tip deflection values whereas the third case favours the system with low tip deflection values. In first case, the highest value of tip deflection is 9.5 degrees and in second case, the highest value is 9.1 degrees.

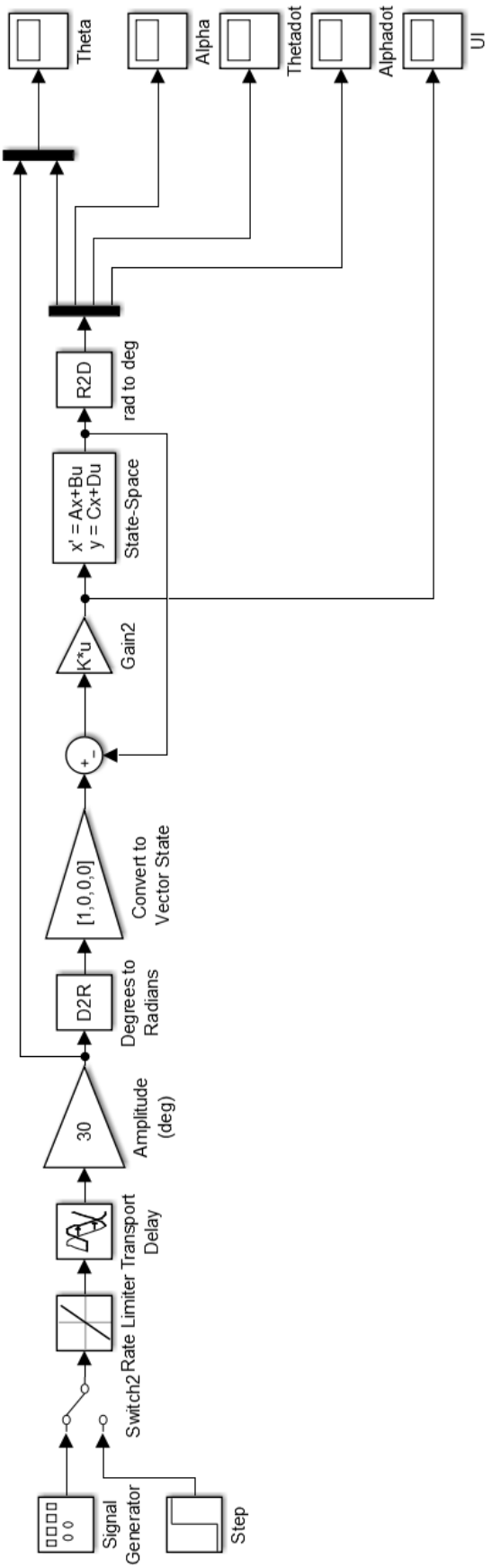

Figure 6.7: Simulink diagram of LQR controller

However, in third case, when Genetic Algorithm based weight matrices are used, the tip deflection is 7.9 degrees. It is also noticed that first and second case have almost same but high settling time of 1.1 seconds. However, in case third, the settling time is 0.57 seconds which is quite low than the first two cases.

It is concluded from Figure 6.6 and Figure 6.7 that the case where weight matrices are selected by Genetic Algorithms supports better results than the other two cases.

In Figure 6.8, comparative study for the shaft angle is done between simulation and experimental response with respect to the reference trajectory. The reference trajectory used here is square wave having same parameters as stated in Figure 6.9. It is observed that both simulation and real-time response show analogous behaviour during the transient phase. As the time elapses, real-time response is lagging by 2 degrees in comparison with the simulation response. This much delay is expected in the experimental results, as the simulation results does not include the effects of unmodeled dynamics like friction and backlash.

In Figure 6.10, comparative study for tip deflection is shown between simulation and and real-time response. It is inferred from the figure that both responses behave in approximately same manner.

It is concluded from Figure 6.10 and Figure 6.11 that both real-time and simulation response follows one another in approximately similar fashion. Therefore, the LQR controller is robust to parametric uncertainties.

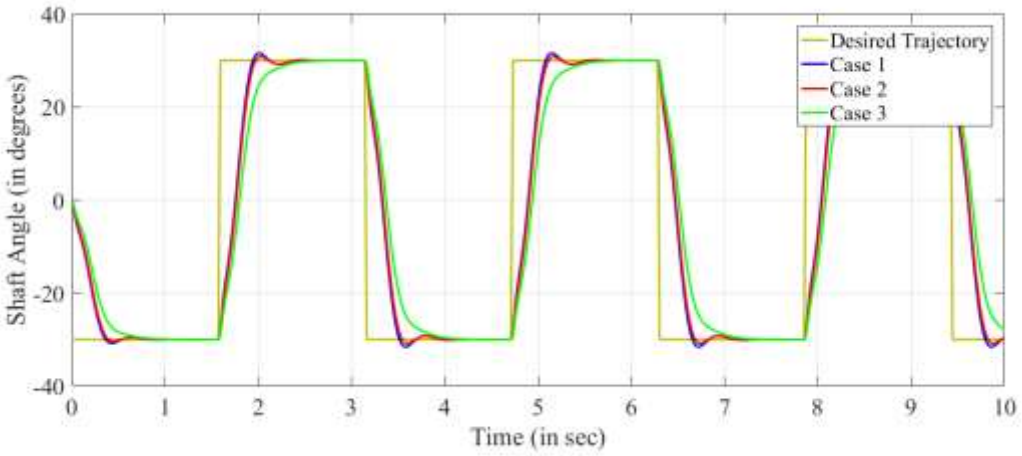

Figure 6.8: Case study of LQR for shaft angle with time.

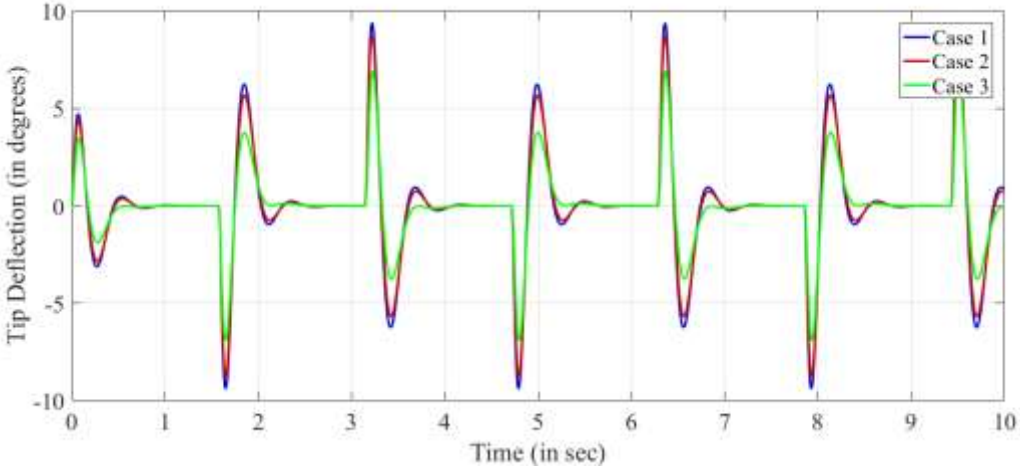

Figure 6.9: Case study of LQR for tip deflection with time.

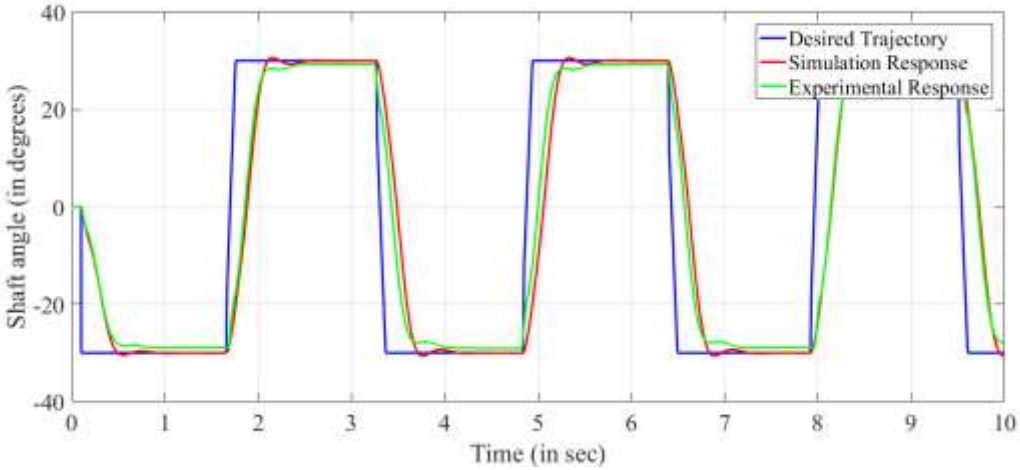

Figure 6.10: Comparison of experimental vs simulation results of shaft angle variation with time using a LQR controller.

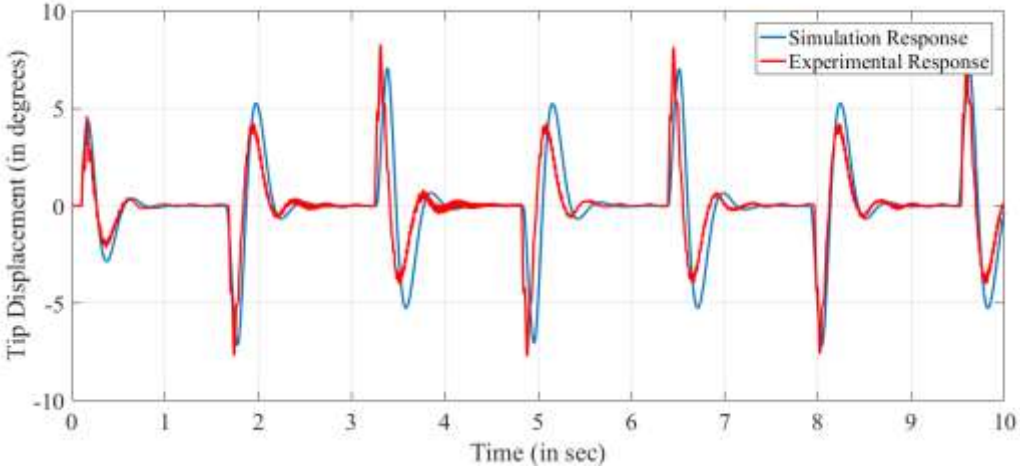

Figure 6.11: LQR comparison of experimental and simulation results for tip deflection

6.5. LQR and Integral Sliding Mode Controller (ISMC) with Input Disturbance

In this section, input disturbance is given to the LQR system with the frequency of 2 Hz and amplitude of 0.5 units as a modification in the Simulink diagram shown in Figure 6.7. The same disturbance is given to the integral sliding mode system as shown in Simulink diagram of Figure 6.12. The gain of ISMC is same as in case 3 of LQR, projection matrix $\boldsymbol{G} = [0,0,0.0081373, -0.0081373]$ and $M_0 = 2.5$. Calculated from Equation 4.16.

Figure 6.13 represents details of sub system integral sliding mode control. Working of integral sliding mode control is discussed in Chapter 4. Experimental model is design to measure shaft angle and tip deflection only. Angular velocity of the shaft and tip deflection velocity is calculated by usage of high gain observer as shown in Figure 6.14. A detail of sub system of scopes is illustrated in Figure 6.15.

In Figure 6.16 and Figure 6.17, the comparative analysis of the simulation response is presented for the shaft angle and tip deflection, respectively. In Figure 6.16, comparative analysis of the LQR controller and ISMC for the shaft angle is presented with reference trajectory. The inference drawn from the figure is that LQR controller provides the variation in shaft angle and does not cooperate with input disturbance whereas the integral sliding mode controller supports better results by showing fewer deviations for shaft angle values. In Figure 6.17, comparative analysis of both the controllers for tip deflection is illustrated. It is noticed from the figure, ISMC supports better results by showing lesser variations of tip angle values than LQR controller.

In Figure 6.18 and Figure 6.19, the comparative analysis for shaft angle and tip deflection is presented with real-time (RT) model. It is concluded from Figures 6.16 – 6.19 that ISM Controller is more robust to input disturbances than LQR controller.

In Figure 6.20, comparative study for shaft angle with ISMC is presented between simulation response and real-time response. It is observed that response of state-space model and real time model is very much similar in transient and steady state both.

In Figure 6.21, comparative study for tip deflection with ISMC is presented between the simulation and experimental results. It is observed that response of state-space model and real-time model is quite similar in transient and steady state both. However, chattering comes into the picture for real-time model, which does not have any significant effect on the results.

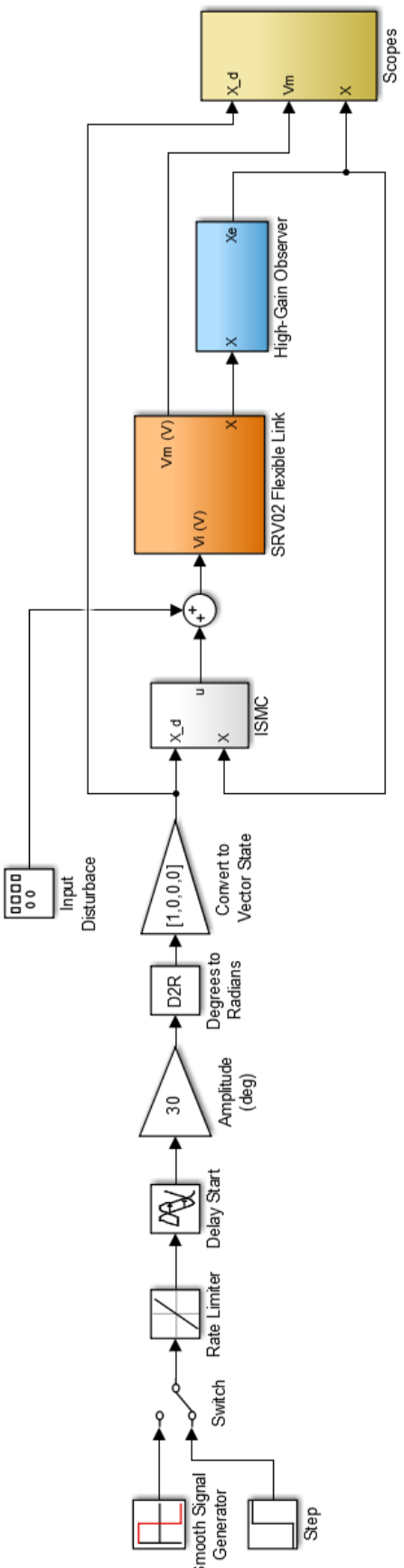

Figure 6.12: Simulink model of integral sliding mode with input disturbance.

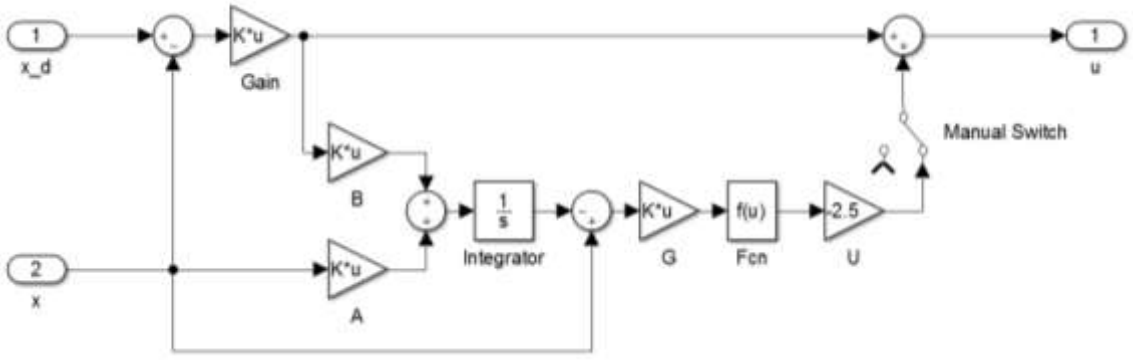

Figure 6.13: Details of Simulink subsystem of integral sliding mode control

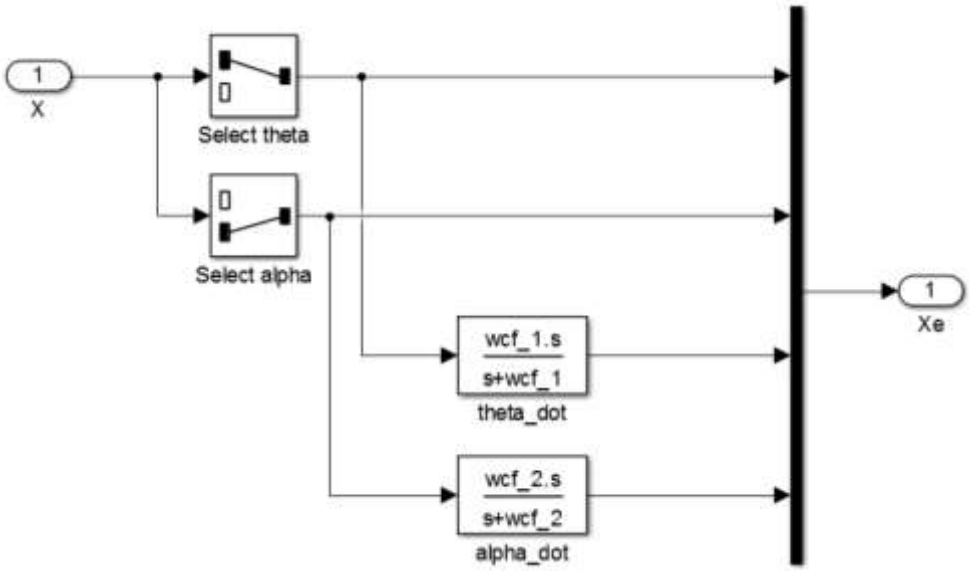

Figure 6.14: Details of Simulink subsystem of high-gain observer

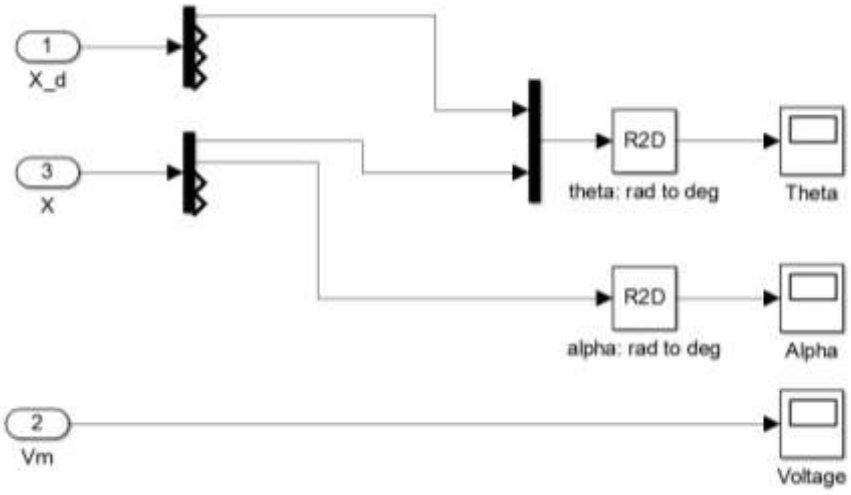

Figure 6.15: Details of Simulink subsystem of scopes

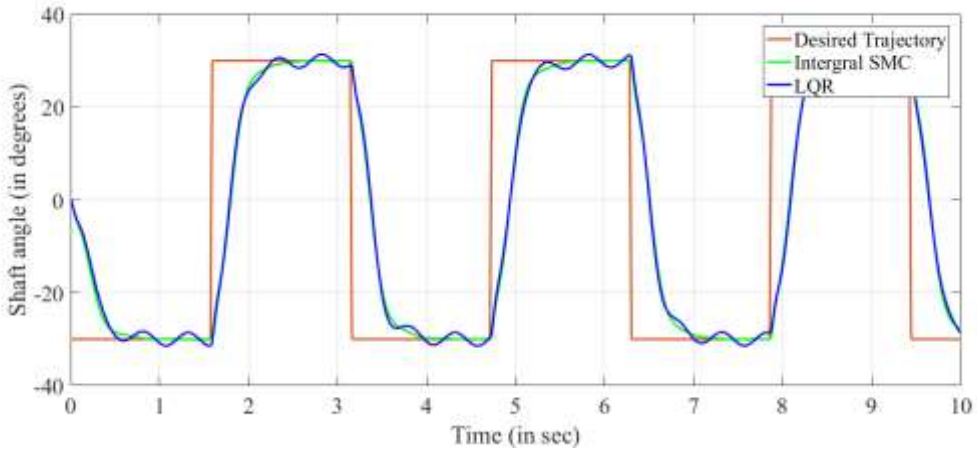

Figure 6.16: Comparison of simulation results using LQR and ISMC controllers for the variation in the shaft angle to input disturbance.

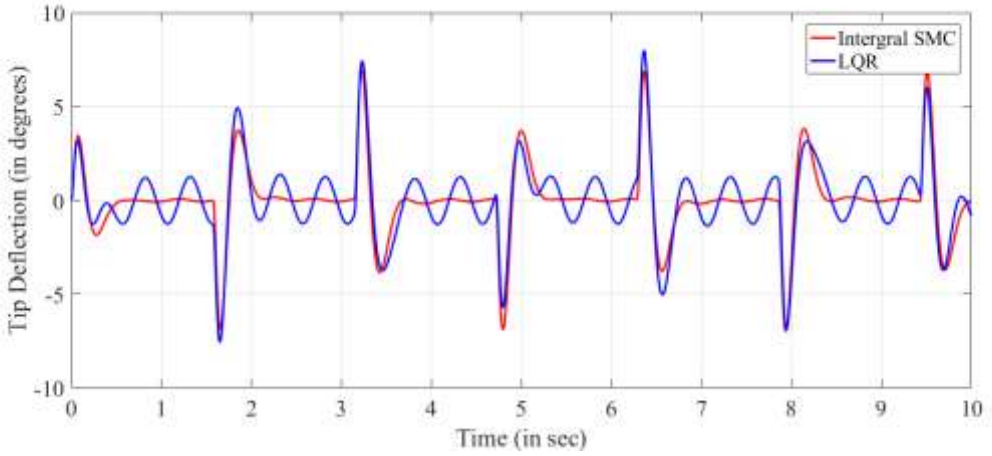

Figure 6.17: Comparison of simulation results using LQR and ISMC controllers for the variation in the tip deflection to input disturbance.

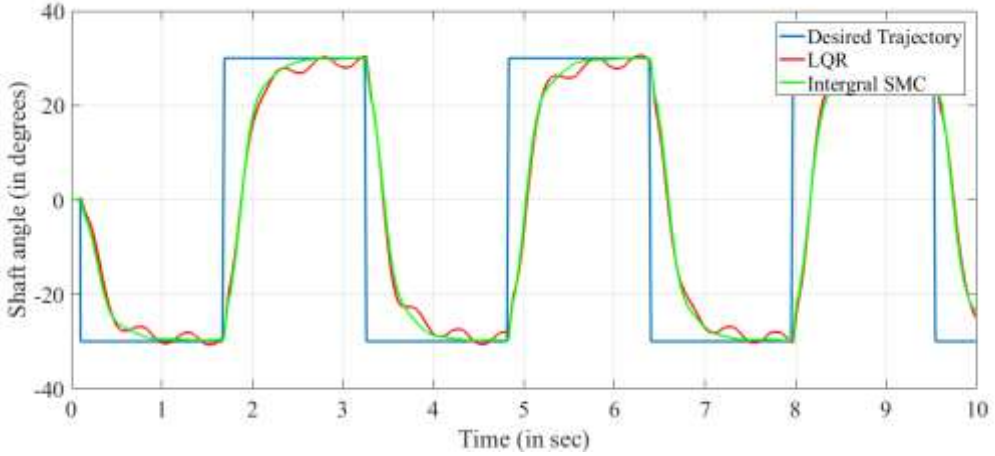

Figure 6.18: Comparison of experimental results using LQR and ISMC controllers for the variation in the shaft angle to input disturbance.

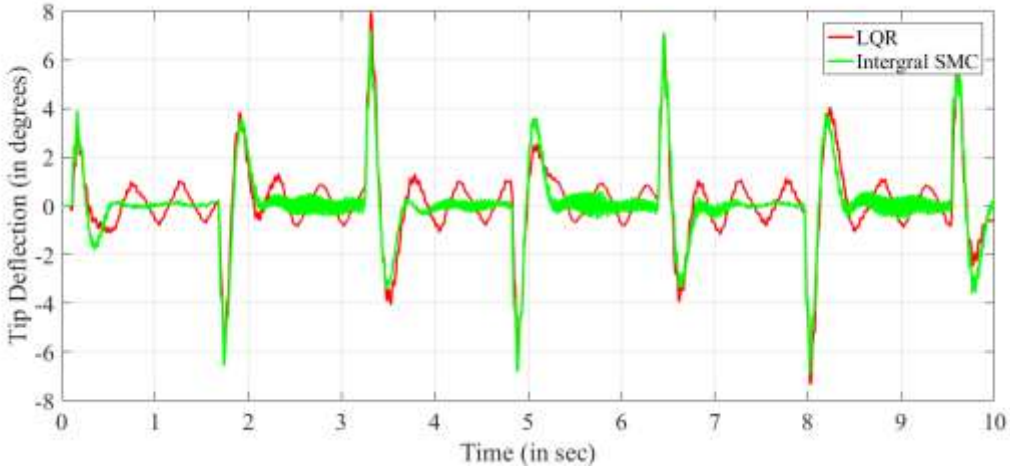

Figure 6.19: Comparison of experimental results using LQR and ISMC controllers for the variation in the tip deflection to input disturbance.

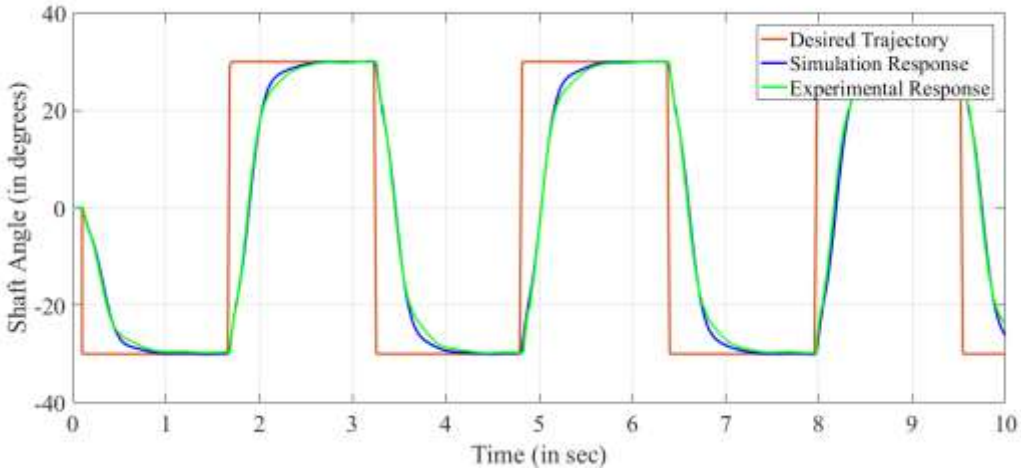

Figure 6.20: ISM controller based comparison of simulation and experimental responses of the shaft angle.

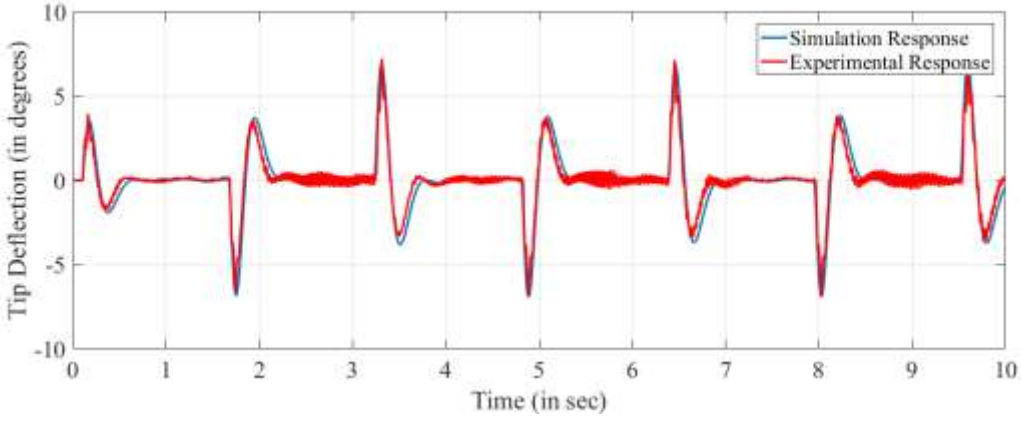

Figure 6.21: ISM controller based comparison of simulation and experimental responses of the tip deflection.

6.6. Summary

In this chapter, the response of both the mathematical models (finite-element model and lumped-parameter model) are compared with the real-time model. It has been observed that the response of both of models matches with the response of real-time model in transient phase and slight discrepancies are found in the steady state. It has also been demonstrated that the Genetic algorithm based LQR gives better results than conventional LQR. Finally, It has been well demonstrated and concluded that the integral sliding mode control is more robust to parametric uncertainties and to input disturbance as compared to the LQR controller

Chapter 7

Conclusions and Future Scopes

7.1. Conclusions

From the current work, the following conclusions can be drawn:

- To develop the dynamic model of flexible manipulators, broadly three type of models are used by researchers, i.e. finite element model, lumped parameter model and assumed mode model. Most of the researchers have been worked on the linear tip deflection using these three models and they had not concentrated on angular tip deflection. Limited work in domain of ISMC had been reported by researchers.
- The precise model of the flexible system plays a vital role in the controller design. In this thesis, two methods have been used for modeling the flexible manipulator i.e. finite element method and lumped parameter model. In finite element method, the linear tip deflection has been considered and in lumped parameter model angular tip deflection has been considered. Modeling of both the methods has been done by using Euler-Lagrange approach. Actuator dynamics has been augmented with both the models. Validation of mathematical model has been done by comparing the shaft angle and tip deflection response to step input with the experimental response of the single link flexible link. From comparison, it has been found that both models track the experimental flexible link very well during the transient phase while some discrepancies are there during steady-state phase.
- Later, in this thesis, the frequency variation analysis has been reported by varying the different parameters associated with the manipulator such as mass of the manipulator, length of the manipulator, flexural rigidity and payload of the manipulator. It has been noticed that the frequency increases with increase in flexural rigidity and decrease in mass, length and payload of the manipulator.
- Parameter uncertainties always exist in the mathematical model. So, robust controller is required to address the parametric uncertainties. Therefore, in this thesis work, two controllers i.e. LQR controller and ISMC have been implemented. Gain of both the controllers has been found by optimizing the weight matrices using Genetic Algorithms. Furthermore, the comparative analysis has been carried out between LQR

and ISMC by applying input disturbances. Moreover, the simulation results in different cases have been validated with the corresponding experimental results. From this, it has been concluded that ISMC confirms better performance than LQR for robustness to parametric uncertainties and input disturbance.

7.2. Future work

On the basis of literature survey and the work done in this dissertation, work on following areas can be done in future:

- Improvement in mathematical modeling of the flexible manipulator could be achieved by considering Coulomb friction at shaft and mass of the wire attached with strain gauge connector of the flexible manipulator. Furthermore, lumped parameter model could be improved by considering more number of element..
- Finite element model could be used to design the controller for flexible link setup with the help of a reduce order observer. Kalman filter could also be used for finding the slope of flexible link whose sensor is not available and reduce the noises in output. Furthermore, Kalman filter can also be used to design controller with finite element model.
- GA based optimization could be explored more by using different performance indexes and different fitness functions.
- Hybrid controller could also be designed for flexible link manipulator by using GA based LQR and ISMC with feedback and command shaping with feedforward, for better control of tip deflection in flexible manipulator.
- Controller, illustrated in this study, could also be designed for flexible manipulator having more number of degrees of freedom.
- Results of variation of natural frequency with the properties and dimension of flexible link could be validated by the using real-time apparatus or lumped parameter model.

References

[1] W. J. Book, “Modeling, design, and control of flexible manipulator arms: a tutorial review,” *29th IEEE Conf. Decis. Control*, vol. 2, pp. 500–506, 1990.

[2] R. H. Cannon and E. Schmitz, “Initial experiments on the end-point control of a flexible one-link robot,” *Int. J. Rob. Res.*, vol. 3(3), pp. 62–75, 1984.

[3] M. Uchiyama, A. Konno, and M. Labora, “Development of flexible dual-arm manipulator tested for space robotics,” in *Proceedings of IEEE International Workshop on Intelligent Robots and System*, pp. 375–381, 1990.

[4] M. A. Meggiolaro and S. Dubowsky, “Improving the positioning accuracy of powerful manipulators with application in nuclear maintenance,” in *Proceedings of the 16th Brazilian Congress of Mechanical Engineering, (COBEM) on Robotics and Control*, pp. 210–219, 1996.

[5] R. Kumar *et al.*, “Preliminary experiments in cooperative human/robot force control for robot assisted microsurgical manipulation,” in *Proceedings of the IEEE International Conference on Robotics and Automation*, pp. 1–8, 2000.

[6] T. Fukuda and Y. Kuribayashi, “Flexibility control of elastic robotic arms and its application to contouring control,” *IEEE Pap. no CH2008-1/84*, pp. 540–545, 1984.

[7] G. Hastings and W. Book, “A linear dynamic model for flexible robotic manipulators,” *IEEE Control Syst. Mag.*, vol. 7(1), pp. 61–64, 1987.

[8] S. K. Dwivedy and P. Eberhard, “Dynamic analysis of flexible manipulators, a literature review,” *Mech. Mach. Theory*, vol. 41(7), pp. 749–777, 2006.

[9] C. T. Kiang, A. Spowage, and C. K. Yoong, “Review of control and sensor system of flexible manipulator,” *J. Intell. Robot. Syst. Theory Appl.*, vol. 77(1), pp. 187–213, 2015.

[10] L. J. Won, J. D. Huggins, and J. B. Wayne, “Experimental verification of a large flexible manipulator,” in *American Control Conference, 1988. IEEE*, pp. 1021–1028, 1988.

[11] F. Bellezza, L. Lanari, and G. Ulivi, “Exact modeling of the flexible slewing link,” *Proceedings., IEEE Int. Conf. Robot. Autom.*, pp. 734–739, 1990.

[12] R. J. Theodore and A. Ghosal, “Comparison of the assumed modes and finite element models for flexible multilink manipulators,” *Int. J. Rob. Res.*, vol. 14(2), pp. 91–111, 1995.

[13] F. Matsuno, S. Noriaki, and I. Masao, “Optimal handling strategies of flexible beams by using n-link manipulators,” *Trans. Soc. Instrum. Control Eng.*, vol. 30(12), pp. 1521–1528, 1994.

[14] F. Karray, S. Tafazolli, and W. Gueaieb, “Robust tracking of a lightweight manipulator system,” *Nonlinear Dyn.*, vol. 20(2), pp. 169–179, 1999.

[15] E. Barbieri and U. Ozguner, “Unconstrained and constrained mode expansions for a flexible slewing link,” *J. Dyn. Syst. Meas. Control*, vol. 110, pp. 416–421, 2016.

[16] F. Rakhsha and A. A. Goldenberg, “Dynamics modelling of a single-link flexible robot,” in *Proceedings of the IEEE International Conference on Robotics and Automation*, pp. 984–989, 1985.

[17] S. S. Ge, T. H. Lee, and G. Zhu, “Improving regulation of a single-link flexible manipulator with strain feedback,” *IEEE Trans. Robot. Autom.*, vol. 14(1), pp. 179–185, 1998.

[18] D. W. Raboud, A. W. Lipsett, M. G. Faulkner, and J. Diep, “Stability evaluation of very flexible cantilever beams,” *Int. J. Non. Linear. Mech.*, vol. 36(7), pp. 1109–1122, 2001.

[19] S. M. Megahed and K. T. Hamza, “Modeling and simulation of planar flexible link manipulators with rigid tip connections to revolute joints,” *Robotica*, vol. 22, pp. 285-300, 2004.

[20] D. Popescu, D. Sendrescu, and E. Bobasu, “Modelling and robust control of a flexible beam Quanser experiment,” *Acta Montan. Slovaca*, vol. 13(1), pp. 127–135, 2008.

[21] W. Khalil and M. Gautier, “Modeling of mechanical systems with lumped elasticity,” in *Proceedings of the IEEE International Conference on Robotics and Automation*, no. 4, pp. 3964–3969, 2000.

[22] D. Nissing, “A vibration damped flexible robot: identification and parameter optimization,” *in Proceedings of the American Control Conference, Chicago, Illinois*, pp. 1715–1719, 2000.

[23] P. B. Usoro, R. Nadira, and S. S. Mahil, “A finite element/lagrange approach to modeling lightweight flexible manipulators,” *J. Dyn. Syst. Meas. Control*, vol. 108(3), pp. 198–205, 1986.

[24] M. O. Tokhi, Z. Mohamed, and A. K. M. Azad, “Finite difference and finite element approaches to dynamic modelling of a flexible manipulator,” *Proc. Inst. Mech. Eng. Part I J. Syst. Control Eng.*, vol. 211(1), pp. 145–156, 1997.

[25] M. O. Tokhi and Z. Mohamed, “Finite element approach to dynamic modelling of a flexible robot manipulator : performance evaluation and computational requirements,” *Commun. Numer. Meth. Eng.*, vol. 678, pp. 669–678, 1999.

[26] Z. Mohamed, J. M. Martins, M. O. Tokhi, J. Sá da Costa, and M. A. Botto, “Vibration control of a very flexible manipulator system,” *Control Eng. Pract.*, vol. 13(3), pp. 267–277, 2005.

[27] Z. Mohamed and M. O. Tokhi, “Command shaping techniques for vibration control of a flexible robot manipulator,” *Mechatronics*, vol. 14(1), pp. 69–90, 2004.

[28] A. Singla, A. Tewari, and B. Dasgupta, “Vibration suppression during input tracking of a flexible manipulator using a hybrid controller,” *Sadhana - Acad. Proc. Eng. Sci.*, vol. 40(6), pp. 1865–1898, 2015.

[29] A. Singla, A. Tewari, and B. Dasgupta, “Command shaped closed loop control of flexible robotic manipulators,”*J. Vib. Eng. Tech.*, vol. 4(2), pp97-110, 2016.

[30] S. Nagarajan and D. A. Turcic, “Lagrangian formulation of the equations of motion for elastic mechanisms with mutual dependence between rigid body and elastic motions. part II : system equations,” *ASME J. Dyn. Syst. Meas. Control*, vol. 112(2), pp. 215–224, 2015.

[31] T. E. Alberts and Y. Chen, “Dynamic analysis to evaluate wiseoelastic passive damping augmentation for the space shuttle remote manipulator system,” *ASME J. Dyn. Syst. Meas. Control*, vol. 114, pp. 68–474, 2016.

[32] K. J. Park, “Flexible robot manipulator path design to reduce the endpoint residual vibration under torque constraints,” *J. Sound Vib.*, vol. 275(3), pp. 1051–1068, 2004.

[33] A. Abe, “Trajectory planning for residual vibration suppression of a two-link rigid-flexible manipulator considering large deformation,” *Mech. Mach. Theory*, vol. 44(9), pp. 1627–1639, 2009.

[34] Y. Choi, J. Cheong, and H. Moon, “A trajectory planning method for output tracking of linear flexible systems using exact equilibrium manifolds,” *IEEE/ASME Trans. Mechatronics*, vol. 15(5), pp. 819–826, 2010.

[35] S. Rhim and W. J. Book, “Adaptive time-delay command shaping filter for flexible manipulator control,” *IEEE/ASME Trans. Mechatronics*, vol. 9(4), pp. 619–626, 2004.

[36] G. Song, S. P. Schmidt, and B. N. Agrawal, “Experimental robustness study of positive position feedback control for active vibration suppression,” *J. Guid. Control. Dyn.*, vol. 25(1), pp. 179–182, 2002.

[37] R. Orszulik and J. J. Shan, “Multi-mode adaptive positive position feedback: An experimental study,” *2011 Am. Control Conf.*, pp. 3315–3319, 2011.

[38] K. Gurses, B. J. Buckham, and E. J. Park, “Vibration control of a single-link flexible manipulator using an array of fiber optic curvature sensors and PZT actuators,” *Mechatronics*, vol. 19(2), pp. 167–177, 2009.

[39] G. Zhu, S. S. Ge, and T. H. Lee, “Simulation studies of tip tracking control of a single-link flexible robot based on a lumped model,” *Robotica*, vol. 17, pp. 71–78, 1999.

[40] P. T. Kotnik, K. Ave, and S. Yurkovich, “Acceleration feedback control for flexible manipulator arm,” in *Proceedings of the IEEE International Conference on Robotics and Automation*, pp. 322–323, 1988.

[41] G. Wang and Y. Li, “Integrated sensing and filter design for a single-link flexible manipulator,” in *IEEE Transactions on Robotics and Automation*, vol. 1(20), pp. 559–564, 2004.

[42] J. Y. Lew and W. J. Book, “Hybrid control of flexible manipulators’ with multiple contacts,” in *IEEE Robotics and Automation Conference*, pp. 242–247, 1993.

[43] M. Z. M. Zain, M. O. Tokhi, and Z. Mohamed, “Hybrid learning control schemes with input shaping of a flexible manipulator system,” *Mechatronics*, vol. 16(4), pp. 209–219, 2006.

[44] S. Lee and C. Lee, “Hybrid control scheme for robust tracking of two-link flexible manipulator,” *J. Intell. Robot. Syst.*, vol. 32(4), pp. 389–410, 2001.

[45] V. Etxebarria, A. Sanz, and I. Lizarraga, “Real-time experimental control of a flexible robotic manipulator using a composite approach,” *Proc. 2004 IEEE Int. Conf. Control*

Appl. 2004., pp. 955–960, 2004.

[46] M. Khairudin, Z. Mohamed, and A. R. Husain, "Dynamic model and robust control of flexible link robot manipulator," *Telkomnika*, vol. 9(2), pp. 279–287, 2011.

[47] L. Meirovitch and R. Parker, *Fundamentals of Vibrations*. Waveland Press, 2001.

[48] V. Utkin, J. Guldner, and J. Shi, *Sliding Mode Control in Electro-Meachanical Systems*. CRC press, 2009.

[49] S. Suklabaidya, K. Lochan, and B. K. Roy, "Control of rotational base single link flexible manipulator using different SMC techniques for variable payloads," *2015 Int. Conf. Energy, Power Environ. Towar. Sustain. Growth, ICEPE 2015*, 2016.

[50] Q. Inc, *Flexible Link User Manual*. 2009.

[51] Q. Inc, *SRV02 User Manual*. 2009.

Web References

W1. https://waowtech.com/wp-content/uploads/2015/06/Bulle-Arm-2.jpg(Last accessed on 16-7-2017)

W2. https://upload.wikimedia.org/wikipedia/commons/thumb/0/02/STS-114_robot_arm_extension.jpg/682px-STS-114_robot_arm_extension.jpg(Last accessed on 16-7-2017)

W3. http://www.quartus.com/wp-content/uploads/figure_1.jpg (Last accessed on 16-7-2017)

W4. http://what-when-how.com/wp-content/uploads/2012/06/tmp589619_thumb.png (Last accessed on 16-7-2017)

W5. http://computationalnonlinear.asmedigitalcollection.asme.org/data/Journals/JCNDDM/927599/cnd_009_01_011014_f001.png(Last accessed on 16-7-2017)

Amardeep_801584003

ORIGINALITY REPORT

%12	%5	%9	%4
SIMILARITY INDEX	INTERNET SOURCES	PUBLICATIONS	STUDENT PAPERS

PRIMARY SOURCES

1	ASHISH SINGLA, ASHISH TEWARI, BHASKAR DASGUPTA. "Vibration suppression during input tracking of a flexible manipulator using a hybrid controller", Sadhana, 2015 Publication	%3
2	Dwivedy, S.K.. "Dynamic analysis of flexible manipulators, a literature review", Mechanism and Machine Theory, 200607 Publication	%1
3	en.wikipedia.org Internet Source	%1
4	www.sakop.pl Internet Source	<%1
5	www.enformatika.org Internet Source	<%1
6	www.ide.iitkgp.ernet.in Internet Source	<%1
7	SINGLA, ASHISH; TEWARI, ASHISH and DASGUPTA, BHASKAR. "Vibration suppression	<%1

	during input tracking of a flexible manipulator using a hybrid controller", Sadhana, 2015. Publication	
8	Submitted to VIT University Student Paper	<%1
9	www.slideshare.net Internet Source	<%1
10	ir.computing.edgehill.ac.uk Internet Source	<%1
11	uir.unisa.ac.za Internet Source	<%1
12	www.coursehero.com Internet Source	<%1
13	Kumar, Abhishek, Sudeep Sharma, and R. Mitra. "Design of Type-2 Fuzzy Controller based on LQR Mapped Fusion Function", International Journal of Intelligent Systems and Applications, 2012. Publication	<%1
14	open.library.ubc.ca Internet Source	<%1
15	Submitted to Coventry University Student Paper	<%1
16	www.soybase.org Internet Source	<%1

17	Mohamed, Z.. "Command shaping techniques for vibration control of a flexible robot manipulator", Mechatronics, 200402 Publication	<%1
18	Submitted to Griffth University Student Paper	<%1
19	Submitted to Technische Universiteit Delft Student Paper	<%1
20	Debbouche, Amar, and Juan J. Nieto. "Sobolev type fractional abstract evolution equations with nonlocal conditions and optimal multi-controls", Applied Mathematics and Computation, 2014. Publication	<%1
21	www.rroij.com Internet Source	<%1
22	Bose, Sujit K., and Ganesh C. Gorain. "Energy Estimate of Boundary Controlled Vibrating Hybrid Structure Subject to Uncertain Forces", Journal of Aerospace Engineering, 2003. Publication	<%1
23	Zhao, Y.. "Dynamics analysis and characteristics of the 8-PSS flexible redundant parallel manipulator", Robotics and Computer Integrated Manufacturing, 201110 Publication	<%1

24	umpir.ump.edu.my Internet Source	<%1
25	Yan-Bin Zhao. "A Real-Time Architecture for Nids Based on Sequence Analysis", 2005 International Conference on Machine Learning and Cybernetics, 2005 Publication	<%1
26	Tanguy, Jean-Michel. "Engineering Model and Real-Time Model", Numerical Methods Tanguy/Numerical Methods, 2013. Publication	<%1
27	Submitted to Swinburne University of Technology Student Paper	<%1
28	S. A. Bochkarev. "Numerical modelling of the stability of loaded shells of revolution containing fluid flows", Journal of Applied Mechanics and Technical Physics, 03/2008 Publication	<%1
29	Submitted to Asian Institute of Technology Student Paper	<%1
30	N. Azizi. "Hybrid simulated annealing with memory: an evolution-based diversification approach", International Journal of Production Research, 08/27/2009 Publication	<%1

31	Submitted to University of Sheffield Student Paper	<%1
32	Submitted to University of Salford Student Paper	<%1
33	Submitted to University of Newcastle upon Tyne Student Paper	<%1
34	ubm.opus.hbz-nrw.de Internet Source	<%1
35	ftp.sco.com Internet Source	<%1
36	Shawky, Alaa, Dawid Zydek, Yehia Z. Elhalwagy, and Andrzej Ordys. "Modeling and nonlinear control of a flexible-link manipulator", Applied Mathematical Modelling, 2013. Publication	<%1
37	Kumar P., Ramesh, Asif Chalanga, and B. Bandyopadhyay. "Smooth integral sliding mode controller for the position control of Stewart platform", ISA Transactions, 2015. Publication	<%1
38	Tuan-Anh Nguyen. "Application of Optimization Methods to Controller Design for Active Suspensions", Mechanics Based Design of Structures and Machines, 7/2007 Publication	<%1

39	Renato Silveira. "Managing coherent groups", Computer Animation and Virtual Worlds, 2008 Publication	<%1
40	www.dtic.mil Internet Source	<%1
41	dspace.lboro.ac.uk Internet Source	<%1
42	eprints.utm.my Internet Source	<%1
43	Chun-shan Lai. "Vector control of induction motor based on online identification and ant colony optimization", 2010 2nd International Conference on Industrial and Information Systems, 07/2010 Publication	<%1
44	"Communication Availability in Communications-Based Train Control Systems", Advances in Communications-Based Train Control Systems, 2015. Publication	<%1
45	Rob van Gils. "Feedback stabilization of transition boiling states", 2010 12th IEEE Intersociety Conference on Thermal and Thermomechanical Phenomena in Electronic Systems, 06/2010 Publication	<%1

46	Zhao, Guoliang. "Fractional-order fast terminal sliding mode control for a class of dynamical systems.(Research Artic", Mathematical Problems in Engineering, Annual 2014 Issue Publication	<%1
47	www.sersc.org Internet Source	<%1
48	Mechatronics by Bond Graphs, 2003. Publication	<%1
49	R C Mohanty. "Investigation into the dynamics of layered and jointed cantilevered beams", Proceedings of the Institution of Mechanical Engineers Part C Journal of Mechanical Engineering Science, 01/01/2010 Publication	<%1
50	M. Nataraju. "Nonlinear Dynamical Effects and Observations in Modeling and Simulating Damage Evolution in a Cantilevered Beam", Structural Health Monitoring, 09/01/2005 Publication	<%1

EXCLUDE QUOTES ON

EXCLUDE BIBLIOGRAPHY ON

EXCLUDE MATCHES < 8 WORDS